Research Square

Preprints are preliminary reports that have not undergone peer review.
They should not be considered conclusive, used to inform clinical practice,
or referenced by the media as validated information.

Regional and Hormone-Associated Adaptations of Tissue-Resident Memory T cells across the Human Female Reproductive Tract.

Alison Kohlmeier

askohlm@emory.edu

Emory University School of Medicine https://orcid.org/0000-0002-7237-1826

Elizabeth Collins

Emory University School of Medicine

Mark Williams

Emory University School of Medicine https://orcid.org/0000-0001-8271-3394

Paola Vidal

Emory University School of Medicine

Sakeenah Hicks

Emory University

Kwoineh Haba

Emory University School of Medicine

Cameron Mattingly

University of Cambridge

Christopher Scharer

Emory University https://orcid.org/0000-0001-7716-8504

Edward Pearce

Johns Hopkins University

Toni Darville

University of North Carolina at Chapel Hill

Jacob Kohlmeier

Emory University School of Medicine

Richa Varughese

Emory University School of Medicine

Article

Keywords:

Posted Date: November 2nd, 2026

DOI: https://doi.org/10.21203/rs.3.rs-11387827/v1

License: This work is licensed under a Creative Commons Attribution 4.0 International License.
Read Full License

Additional Declarations: There is **NO** Competing Interest.

Regional and Hormone-Associated Adaptations of Tissue-Resident Memory T cells across the Human Female Reproductive Tract.

Elizabeth M.B. Collins[1,6], Richa S. Varughese[2,6], M. Elliott Williams[2], Paola Vidal[2], Sakeenah L. Hicks[2], Kwoineh J. Haba[1], Cameron L.R. Mattingly[2], Christopher D. Scharer[2], Edward J. Pearce[3,4], Toni Darville[5], Jacob E. Kohlmeier[2], & Alison Swaims-Kohlmeier[1,2,*]

[1]The Department of Gynecology and Obstetrics, Emory University School of Medicine, Atlanta, Georgia, U.S.A.
[2]The Department of Microbiology and Immunology, Emory University School of Medicine, Atlanta, Georgia, U.S.A.
[3] The Bloomberg Kimmel Institute and Department of Oncology, Johns Hopkins University School of Medicine, Baltimore, Maryland, U.S.A.
[4]The Department of Molecular Microbiology and Immunology, Johns Hopkins University Bloomberg School of Public Health, Baltimore, Maryland, U.S.A.
[5]The Department of Pediatrics, University of North Carolina at Chapel Hill, Chapel Hill, North Carolina, U.S.A.
[6]*These authors contributed equally*
[*]*Corresponding author: askohlm@emory.edu*

Abstract: Tissue-resident memory T cells (TRM) are essential components of mucosal immunity, yet their organization and regulation across the human female reproductive tract (FRT) remain poorly understood. Here, we investigated TRM across the FRT from donors with diverse hormonal profiles and identified regional and lineage-specific differences in phenotype, transcriptional programming, and abundance. CD8 T cells displayed greater enrichment of canonical TRM signatures and extensive T cell receptor clonal sharing across tissues, suggesting a common antigenic immune history. Despite these differences, resident CD4 and CD8 T cells shared CCR5 protein expression and *TSC22D3* transcript enrichment, highlighting potentially distinctive features of FRT TRM. Single-cell transcriptomics revealed compartmental differences in metabolic, stress- and hormone-response pathways. Progesterone and testosterone levels were associated with differences in cervical T cell composition and CD8 TRM abundance. Together, these findings describe regional specialization by resident T cell immunity across the FRT and show that hormonal cues contribute to their homeostasis, offering new insight into factors that shape immune surveillance at mucosal sites of urogenital pathogen exposure.

Background:

Tissue-resident memory T cells (TRM) are a specialized subset of long-lived memory T cells within non-lymphoid tissues and are increasingly recognized as critical mediators of barrier immunity, where they can provide rapid immune protection at mucosal surfaces[1-7]. TRM share core molecular and transcriptional signatures that distinguish them phenotypically and functionally from circulating memory T cells, and the local tissue

environment plays an essential role in establishing and maintaining their residency[8,9]. Beyond structural support provided by epithelial cells, stromal/fibroblast cells, and the vasculature, immunometabolic signaling interactions also shape differentiation and persistence. Cytokines, integrins, fatty acids, glucocorticoids, and local antigen availability have all been shown to regulate their homeostasis[10,11]. However, despite well-established impacts of the major sex hormones, estrogen, progesterone, and testosterone, on immune responses to pathogens (both endogenous and exogenous forms)[12-17], the potential influence on tissue-resident T cell biology remains largely unexplored.

The female reproductive tract (FRT) represents a unique mucosal environment, comprising anatomically and functionally distinct regions, including the uterus, endocervix, and ectocervix, that are subject to dynamic hormonal regulation. Both CD4 and CD8 TRM contribute to protection against urogenital pathogens by limiting infection and disease[18], yet the effects of sex hormones on their homeostasis within these tissues remain poorly defined. Thus, addressing this gap is necessary to advance our understanding of mucosal immunity in the FRT and has implications for infection susceptibility, reproductive health, and therapeutic interventions.

Here, we performed cellular and transcriptional immune profiling of CD4 and CD8 T cells across the FRT in reproductive-age donors with defined hormonal status. This approach uncovered lineage- and hormone-specific differences in cell programming across anatomical regions of the FRT. Overall, FRT CD8 T cell populations exhibited greater phenotypic and transcriptional commitment to canonical TRM programs than their CD4 counterparts, although this varied by tissue site. T cell receptor (TCR) sequencing revealed extensive CD8 T cell clonal overlap throughout the FRT, whereas CD4 T cell clonotypes remained compartmentalized. Despite these differences, FRT-resident CD4 and CD8 T cells shared features across tissue regions, including expression of cell-surface CCR5 and enrichment of the glucocorticoid-response gene transcript GILZ (*TSC22D3*). Pathway analysis further described regional and hormone-associated differences in immune function, cellular metabolism, hypoxia, cell-stress responses, and estrogen-response signaling. Sex hormone levels were also associated with variations in FRT-resident T cells. Notably, progesterone and testosterone concentrations were linked with ectocervical CD8 TRM abundance, metabolic fitness, and immune function.

Taken together, this investigation reveals a high degree of clonal sharing among human FRT CD8 T cells across distinct niches and demonstrates that both anatomic location and sex hormones shape their abundance and transcriptional programming within the FRT. These insights provide a context for understanding how sex hormones can influence mucosal T cell-mediated defense and may inform strategies to strengthen immunity against urogenital pathogens.

Results:

Demographics and hormone levels

A total of 16 hysterectomy hemispecimens and matching blood samples were included in this study. Participants were adults assigned female at birth, of reproductive age (mean ±SD: 30 years ±7.96), and had a recent negative Pap test result. Additional eligibility criteria included the absence of recent genital infections or incidental lesions (further described in the materials and methods). This cohort included a high number of participants reporting exogenous hormone therapy use, particularly testosterone (summarized in Supplemental Table 1). Tissues were evaluated by a pathologist for abnormalities that would preclude immune profiling. In some cases, cervical tissue was not provided. Circulating sex hormone levels (both endogenous and exogenous) were measured by mass spectrometry (Table 1). We assessed all immune profiling for potential correlations with sex hormone levels and report significant associations here.

Memory T cell distribution and hormonal associations within FRT tissue regions. To evaluate T cell distribution across anatomic regions of the female reproductive tract (FRT), ectocervical, endocervical, and uterine tissues were processed into single-cell suspensions and then analyzed by flow cytometry (Fig. 1A and Supplemental Fig. 1). We first compared total T cell yields (per gram of tissue; Fig. 1B), which were higher in ectocervical tissue than in endocervical and uterine tissues (5-fold and 6-fold higher, respectively). Regarding sex hormones, uterine T cell numbers trended higher in donors with increased progesterone levels (Fig. 1C); however, Spearman's test did not detect a significant correlation. Comparing T cell frequency (from the leukocyte pool) (Fig. 1D) showed that uterine and endocervical T cells (44.36% ± 10.69 and 44.06% ± 13.72, respectively) were decreased in comparison to peripheral blood mononuclear cells (PBMC: 64.33% ± 10.82), whereas ectocervical tissue (51.32% ± 18) was not significantly different. No trends were detected with hormone levels and T cell frequency. Collectively, these findings identify the ectocervix as a site of increased T cell density across the FRT regions, consistent with prior macaque studies using intravital vascular labeling to distinguish tissue-localized cells[19].

Next, we characterized T cell subtypes by gating on $CD4^+$, $CD8^+$, and $CD4^-$ $CD8^-$ cells across total $CD3^+$ T cells (Fig. 1E). Within each tissue, CD4 and CD8 frequencies were not significantly different, whereas $CD4^-$ $CD8^-$ T cells comprised the smallest fraction across all regions (13.15% ± 7.67; Fig. 1F). In comparison to PBMC, the T cell ratios (CD4:CD8) from all FRT tissues were reduced (1.142 ± 0.624 versus PBMC: 2.612 ± 1.159; Fig. 1G). Hormonal correlations identified a negative association between ectocervical CD4 T cell frequency and testosterone levels (Fig. 1H).

Grouping T cells into memory subsets (Fig. 1I-K) showed that effector memory CD4 and CD8 T cells (TEM: $CD45RA^-$ $CCR7^-$) were the predominant population throughout the

FRT (57.29% ± 23.59 versus PBMC:19.3% ± 13.994), while naïve T cells (TNA: CD45RA$^+$ CCR7$^+$) were substantially reduced (10.16% ± 15.56 versus PBMC: 51.39% ± 18.35). CD4$^-$ CD8$^-$ T cells, however, did not demonstrate these distinctions, with little to no differences in T cell subsets detected between FRT populations and PBMC (Supplemental Fig. 2).

Given the prior identification of FRT-localized T cells with a TCM phenotype, including a population of tissue-localized migratory memory T cells[20], we compared TCM phenotypes in CD4 and CD8 T cells (Fig. 1L). CD4 TCM frequencies from all sites were generally increased compared to CD8 TCM (15.19% ± 12.88 versus CD8: 6.12% ± 6.11), though no difference was detected in endocervical tissue. Comparing CD4 TCM across tissue sites showed that only uterine CD4 TCM frequencies were significantly reduced (15.498% ± 12.735 versus PBMC: 21.5% ± 11.835). In contrast, CD4 and CD8 TEM populations across all FRT tissues were increased, with no differences detected among subsets (Fig. 1M). No correlations between hormone levels and T cell subsets were detected.

Overall, FRT tissues exhibited regional differences in T cell density, greater representation of CD8 T cell subsets, and a predominance of effector phenotypes among both CD4 and CD8 T cells, consistent with previous studies of T cell immune surveillance at peripheral barrier tissues[5,21-23]. Although we did not detect T cell subtype or subset changes in PBMCs, higher circulating testosterone concentrations were associated with lower frequencies of ectocervical CD4 T cells, suggesting that systemic hormone levels may be linked to regional differences in T cell composition.

Resident T cell phenotypes and T cell receptor clonal sharing across the FRT. Next, to assess FRT memory T cell properties associated with their long-lived localization, we evaluated resident T cell phenotypes by measuring surface expression of CD69 and CD103 on CD4 and CD8 TEM populations[24] (Fig 2A). Within CD4 TEM, CD69$^+$ CD103$^-$ single positive TRM (SP) were significantly increased across FRT tissues (mean range ±SD: 45-55.7% ± 13.1 versus PBMC: 3.42% ± 3.34; Fig. 2B), although a modest but significant increase in CD4 CD69$^+$ CD103$^+$ TRM (DP) was also observed (2.73-16.71% ± 9.12 versus PBMC: 0.04% ± 0.09). In contrast, FRT CD8 TEM were more enriched for DP populations (34.46-52.19% ± 23.63 versus PBMC: 0.66% ± 0.89; Fig. 2C); however, SP CD8 populations were also prevalent (25.32-31.8% ± 16.3 versus PBMC: 9.24% ± 6.81). Correspondingly, FRT CD4 and CD8 CD69$^-$ CD103$^-$ double-negative (non-TRM; DN) populations were generally reduced (27.9% ± 15.24 versus PBMC: 89.1% ± 12.87), with the exception of uterine DN CD4 TEM (52.68% ± 12.22%). Analysis of CD4 TCM populations also showed migratory memory T cells (TMM: % CD69$^+$ CD103$^{+/-}$ from TCM) increased across all FRT regions (51.41% ± 40.57 versus PBMCs; 4.4% ± 5.495), with similar frequencies of TMM and DN TCM subsets across sites (Supplemental Fig. 3).

Direct comparison by T cell subtype lineage confirmed that FRT CD4 T cells more frequently displayed a SP phenotype (Fig 2D), whereas FRT CD8 T cells were predominantly DP (Fig 2E), consistent with previous reports[24]. Regionally, ectocervical tissues were more likely to contain DP populations, while uterine tissues were more likely to comprise SP populations. Collectively, these findings indicate tissue- and subset-specific differences in TRM distribution across cervical and uterine compartments.

To investigate the clonal relationship among T cell subsets within and across FRT tissues, we performed single-cell alpha and beta-chain T cell receptor (TCR) sequencing of ectocervical and uterine T cells, stratifying by resident T cell phenotype (Fig 2F). TCR repertoire analysis revealed clonal sharing among both CD8 (18.82%) and CD4 (14.55%) TEM populations, whereas no clonal sharing was detected among CD4 TCM populations (Fig 2G). Within individual tissues, CD4 T cell clonal sharing occurred primarily between SP and DN TEM populations, with no overlap involving TCM populations despite the detection of numerous clonotypes (Fig 2H). In contrast, CD8 T cells exhibited extensive clonal sharing across phenotypic subsets (Fig 2I). In the uterus, the greatest overlap occurred among all three CD8 subsets, followed by sharing between DN and SP populations. In the ectocervix, clonal sharing was most prominent between DN and SP CD8 populations, followed by overlap across all three subsets. In both tissues, sharing restricted to DN and DP subsets was comparatively rare. Analysis of TCR repertoires across anatomical regions further revealed limited sharing among CD4 T cell populations but extensive sharing among CD8 T cell populations between the ectocervix and uterus (Fig 2J).

Overall, these data demonstrate compartment-specific differences in resident T cell phenotypes between ectocervical and uterine tissues. Notably, CD8 T cells, including TRM subsets, showed greater cross-tissue clonal sharing, indicating a common antigen-driven immune history across FRT regions, whereas the CD4 T cell repertoire appeared more compartmentalized.

Cell surface CCR5 is enriched on TRM across the FRT. CCR5 has been previously identified as a marker of CD4 TRM in vaginal and cervical tissues[25], and CCR5 signaling is known to regulate CD4 T cell trafficking into the FRT[19]. To better define CCR5 frequency and distribution across FRT T cell subtypes, we measured cell-surface CCR5 expression on a subgroup of donors (Fig 3A). Among total TEM, CCR5 expression was markedly increased in all FRT tissues compared with PBMC (ECTO 67.25% ± 14.26, ENDO 66.8% ± 14.14, and uterine 54.81% ± 16.77 versus 20.94% ± 7.3) (Fig. 3B). Analysis of CCR5 distribution among TEM within each region showed a general skewing toward CD8 subtypes, although this was only significant in the endocervix (CD8: 55.7% ± 11.73 and CD4: 37.01% ± 14.71) (Fig 3C).

Direct measurement of CCR5 from tissue-resident T cells showed that virtually all CD8 DP populations throughout the FRT were CCR5+ (93.25% ± 7.84) (Fig 3D). Mean CCR5 expression was slightly lower in CD8 SP populations (86.32% ± 11.48), although this difference was not statistically significant. Within CD8 SP populations, uterine CCR5 expression (mean ±SD: 84.56% ± 10.39) was significantly lower than in endocervical SP populations (mean ±SD: 91.74% ± 8.35). Among CD4 subsets, CCR5 expression was also high in DP populations (90.83% ± 12.38), particularly in cervical tissue, where DP populations exhibited significantly higher CCR5 expression than SP populations. Measuring CCR5 on migratory memory T cell populations showed a different pattern (Supplemental Fig. 4). Unlike TRM, TMM exhibited a wide range in CCR5 expression that was not predicted from CD69 or CD103 expression. We detected no associations or trends between CCR5 expression and hormone levels. Together, these findings identify CCR5 as a robust marker of tissue-resident CD4 and CD8 T cell populations throughout the FRT.

Transcriptional profiling identifies subtypic and regional TRM heterogeneities. Next, we performed single-cell RNA sequencing (scRNA-seq) to compare TRM gene profiles within FRT regions. Tissue-resident T cells were annotated in the dataset using the markers CD3D, CD3G, CD4, CD8A, CD8B, CD69, and ITGAE, which showed strong cell-type specificity with few detectable regulatory T cells (0.3% $FOXP3^+$ CD4 T cells).

Beginning with a uniform manifold approximation and projection (UMAP) analysis, discrete clustering patterns by TRM subsets, including CD4 SP, CD4 DP, CD8 SP, and CD8 DP populations, alongside their DN counterparts, were identified (Fig 4A). Overall, a greater number of CD8 T cells were detected compared with CD4 T cells (3.6-fold increase). In the CD4 SP and DP populations, we detected few significant differentially expressed genes (DEGs), with no consistency across donors. In contrast, CD8 subsets demonstrated marked differences, including 19 shared DEGs comparing CD8 SP with DN and 55 shared DEGs comparing CD8 DP with DN. Across tissue-resident T cell populations, we observed enrichment of *FOS*, a recently identified TRM core marker, and *TSC22D3*, which encodes GILZ, a glucocorticoid-induced regulator of immune responses[27,28]. To further define FRT CD8 TRM, we directly compared SP and DP populations and found 15 shared DEGs, including TRM core genes *ITGA1*, *CXCR6*, *RGS1*, and *PDCD1,* enriched in DP population[24].

To specifically assess tissue-resident T cell identity, we compared CD4 and CD8 subsets within the human TRM gene module[29] (Fig 4B). This approach showed that CD4 SP and DP populations failed to exhibit TRM-associated gene downregulation compared with DN populations, although significant enrichment of upregulated TRM core genes was detected in CD4 DP populations compared with both SP and DN populations. Conversely, CD8 DP populations demonstrated module enrichment as compared to SP and DN

populations, while CD8 SP populations were enriched for upregulated TRM core genes as compared with DN cells.

A global DEG mean summary showed that CD8 DP populations exhibited the greatest differences compared with DN populations, followed by SP populations, whereas CD4 TRM subsets showed comparatively few differences (Fig 4C). Similarly, comparison of resident T cell populations by uterine or ectocervical localization revealed minimal differences among CD4 TRM subsets, whereas CD8 TRM subsets displayed more pronounced regional differences, particularly within SP cells.

Dot plot analysis of core TRM-associated genes further revealed distinct subset-specific patterns (Fig 4D). CD8 DP populations most closely matched a canonical TRM phenotype, with enriched TRM-upregulated genes (*ITGA1*, *SPRY1*, *DUSP10*, *ZNF683*, *DUSP4*, *BTG1, KLF6)* and reduced expression of TRM-downregulated genes (*KLF2*, *S1PR5*, *S1PR1*, *SELL*, and *CCR7*). CD8 SP populations exhibited an intermediate profile between DP and DN populations. In contrast to CD8 DP, CD4 DP populations exhibited a more intermediate transcriptional state, notably retaining *KLF2*, a T cell trafficking marker. CD4 SP populations more closely resembled DN cells, with the exception of increased *KLF6* and *FOS* expression. Because resident CD4 and CD8 T cell subsets also showed enrichment patterns with *TSC22D3*, a gene not previously identified as a TRM core marker, we directly examined its expression (Fig 4E). Single-cell transcript measurements confirmed increased *TSC22D3* expression across resident T cell subsets relative to DN populations, with the strongest enrichment observed among CD8 TRM subsets.

Based on the DEG summary (Fig 4C), we next compared TRM between ectocervical and uterine compartments (Fig 4F). Although we detected no DEGs in CD4 DP populations, the SP population showed modest donor-shared DEG enrichment of *KLF2*, *TXNIP*, a regulator of cellular stress responses[30], and *SP100*, an interferon-stimulated gene in uterine tissue. In contrast, resident CD8 T cell subsets showed more pronounced tissue-specific differences, particularly within SP populations (SP: 264 uterine-enriched and 150 ectocervical-enriched; DP: 62 uterine-enriched and 28 ectocervical-enriched). Across subsets, ectocervical TRM were characterized by increased metal-ion homeostasis mediators such as *MT1X* and *MT2A*.

Module scoring from both CD8 subsets revealed differences in TRM commitment based on cell localization (Fig 4G). Both ectocervical CD8 SP and DP subsets demonstrated greater TRM module enrichment than uterine subsets. Gene set enrichment analysis highlighted biological pathways underlying tissue-specific phenotypes (Fig 4H). In CD4 SP populations, ectocervical tissue identified donor-shared pathway enrichment for cellular response to oxidative stress. Within uterine tissues, resident CD8 T cell subsets

were enriched for activation-associated programming, while in ectocervical tissues, resident CD8 T cell subsets were enriched for metal ion and hypoxia response pathways. Ectocervical CD8 SP populations also showed enrichment for TNFα signaling. Overall, these results demonstrate that TRM heterogeneity in the FRT is driven by T cell lineage (CD4 and CD8), differentiation state (SP and DP), and tissue location, with more pronounced differences detected in resident CD8 T cell subsets.

FRT TRM transcriptional programming distinguished by hormone status. To explore whether sex hormone status influenced FRT tissue resident T cell programming, we compared donor gene profiles based on sex hormone status, which varied by progesterone and testosterone (Fig 5A) (Donor A-high progesterone and low testosterone, or Donor B-low progesterone and high testosterone). Beginning with an evaluation of total cell composition, we identified consistent UMAP clustering patterns across major populations (Fig 5B). However, donor stratification revealed substantial changes in ectocervical cell composition (Fig 5C), characterized, in part, by reduced proportions of structural cells, including endothelial cells, fibroblasts, and epithelial cells in Donor B (consistent with testosterone-driven differences at this tissue site[31,32]), resulting in a greater proportion of the T cell-enriched fraction. UMAP visualization of T cell subtypes showed reduced CD4 T cells from Donor B, with moderate differences in clustering patterns in both resident CD4 and CD8 T cells (Fig 5D).

DEG analysis of TRM subsets indicated modest overall reductions from Donor B, while preserving subset- and tissue-specific trends; apart from tissue-specific DEGs detected only in the Donor A CD4 SP population, few to no differences were detected in CD4 TRM (Fig 5E). KEGG analysis of resident CD8 T cell subsets revealed themes from single-cell pathway analysis that distinguished TRM (Fig 5F). In ectocervical tissues, immune function, cell metabolism, and non-estrogen hormone response signaling were enriched in Donor B, whereas Donor A showed increased cell stress and estrogen response signaling. Resident CD8 T cells from uterine tissues showed a similar trend, with subset-specific exceptions in T cell responses, cell metabolism, and non-estrogen hormone response.

Net SCPA scores (Fig 5G) showed that across resident CD8 T cell subsets, higher scores were detected with estrogen response and cell stress pathways in Donor A, whereas in Donor B, the highest scores were specifically related to cell proliferation/cycle, adhesion/migration, and interferon/cytokine signaling. Some subset-specific differences were detected with cell metabolism (further summarized in Supplemental Fig. 5) and activation in uterine CD8 DP populations, which were otherwise higher in Donor B.

Due to the differences in estrogen-response signaling, we further evaluated this pathway by generating heat maps of associated gene expression in CD8 TRM (Fig. 5H). This showed that, despite comparable estrogen levels (49.14 and 51.43 pg/mL, respectively)

among donors, resident CD8 T cells exhibited patterns that varied by subset, tissue site, and donor. Although a greater proportion of genes were detected in CD8 SP populations, stronger expression differences were observed in DP cells, particularly in the ectocervix.

Taken together, these data show that TRM transcriptional analysis by sex hormone status identified compartmental differences in programming between ectocervical and uterine tissues, suggesting greater overall cell-intrinsic fitness in CD8 SP and DP cells under elevated testosterone and reduced progesterone.

Sex hormone associations with cervical T cell composition and abundance. To further investigate the potential relationship between circulating hormone levels and FRT T cell adaptations, we first performed a correlation analysis between estrogen, progesterone, and testosterone concentrations and the frequency of FRT CD4 and CD8 T cell subsets: DN, SP, DP from TEM or TCM to test for differences in cell composition (Fig. 6A and Supplemental Table 2). This resulted in five associations: four correlations with testosterone levels and one correlation with estrogen. Trends with testosterone levels described reduced TMM (SP and DP) frequencies in the ectocervix and CD8 SP populations in the endocervix, while estrogen exhibited one DN (TEM) positive association in the endocervix. Overall, this approach suggested that circulating testosterone levels, and to a lesser extent estrogen, were associated with variations in cervical T cell composition.

Next, we explored potential associations between hormone levels and FRT-resident T cell abundance through correlation analysis with TRM SP and DP cell yields (Fig. 6B). This showed that while estrogen was not significantly associated with CD4 or CD8 TRM yields, higher progesterone levels were associated with reduced ectocervical CD8 DP populations, while higher testosterone levels correlated with increased DP cells.

To further examine these associations, we stratified donors into low (<1 ng/mL) or high (≥ 1 ng/mL) testosterone groups and compared SP and DP resident T cell yields (Fig 6C). Among SP populations, ectocervical CD4 T cells were generally more abundant than their endocervical and uterine counterparts (Fig 6D). CD8 SP populations also exhibited greater mean abundance in the high-testosterone group, although this difference was not statistically significant. Among DP TRM populations, ectocervical CD8 T cell abundance was higher in the high-testosterone group than in the low-testosterone group (258.1 ± 284 versus 35.2 ± 34.2 cells/g, mean ±SD; Fig. 6E). Within the high-testosterone group, ectocervical CD8 DP cells were also more abundant than their endocervical (41.57 ± 70.57), and uterine TRM (24.36 ± 22.45) counterparts. Reported exogenous hormone use did not reliably predict high testosterone levels (Supplemental Table 1). However, donors reporting natural menstrual cycles exhibited the highest progesterone concentrations (Fig. 6F, G) but lower ectocervical CD8 DP cell abundance (21.14 ± 14.44; Fig. 6G).

Collectively, these findings identify associations between circulating sex hormone concentrations and cervical CD8 resident T cell abundance.

Discussion:

Vaccination approaches designed to support long-lived resident T cell populations in the FRT may offer a promising strategy for protecting against severe diseases caused by urogenital pathogens[4,33-35]. Here, we sought to define tissue-resident T cell populations within hormonally regulated environments across FRT tissue regions in a cohort of reproductive-age participants with diverse hormonal states. Our findings reveal that these T cell populations undergo adaptations driven by T cell subtype lineage, tissue location, and sex hormone status.

Consistent with previous studies from barrier tissues such as the lung, gut, and skin, FRT CD8 T cell populations were more committed to canonical TRM-associated programming than CD4 T cell populations[5]; although ectocervical TRM were significantly more enriched for this program, irrespective of lineage. Growing evidence shows that $CD69^+$ TRM (SP) exhibits greater functional plasticity than $CD69^+$ $CD103^+$ TRM (DP)[36]. Supporting this idea, we found that tissue-resident CD4 T cells (predominantly SP) upregulated genes associated with cell-tissue retention but did not exhibit a corresponding reduction in the expression of genes associated with T cell trafficking, including KLF2. Moreover, tissue-resident CD4 T cell populations were phenotypically more likely to express the lymphatic homing chemokine receptor CCR7, particularly in the ectocervix. A growing number of studies find evidence that, within the stratified epithelial layers of epidermal and lower FRT (vaginal and ectocervical) tissues, CD4 T cells are re-entering circulation[19,20,37,38], although it remains unclear whether and how this might contribute to immune protection at these barrier tissues or, alternatively, in the case of HIV exposure from sexual contact, how this might impact infection risk[39,40]. Particularly given that CD4 T cells in the lower FRT, unlike epidermal tissues, are also readily detected at the luminal surface where pathogen exposure occurs[20] and CCR5 protein expression, the primary HIV co-receptor, is a defining feature of these cells[25,41,42].

Analysis of the TCR repertoire showed that CD8 T cells, including TRM subsets, exhibited substantially greater TCR clonal sharing across FRT regions, whereas CD4 T cells remained largely compartmentalized. This disparity may reflect lineage-specific differences in how local antigen regulates TRM generation within the FRT[43]. Conversely, it may reflect the increased trafficking potential of FRT CD4 T cells discussed above, which could result in the gradual loss of related CD4 T cell clones from the tissue. Future studies defining the antigenic specificities of these T cell populations, particularly TRM cells, may therefore provide important insight into how immune responses are regionally organized and maintained within the human FRT and how they contribute to protective immunity[44].

Compartmental profiling revealed that FRT TRMs were shaped by tissue-specific differences, as evidenced by differential detection of transcriptional programs associated with immune function, hypoxia, metal ion responses, and metabolic fitness. Although CD8 SP populations showed the greatest overall differences, both CD4 and CD8 SP populations showed ectocervical enrichment of cellular stress-associated programming. Additionally, both resident CD8 T cell subsets demonstrated greater immune function-associated programming in the uterus, with increased cell stress and hypoxia enriched in the ectocervix. Across CD4 SP populations and all CD8 TRM, these patterns suggest that the ectocervix appears to impose a distinct metabolic and stress-associated environment on TRM despite harboring greater numbers of these cells. This finding is noteworthy because the ectocervix serves as the first line of defense against genital pathogens, where effective local immunity is essential for preventing ascending infection and the subsequent immune-mediated pathology of the upper FRT.

Importantly, ectocervical resident CD8 T cell abundance was negatively associated with circulating progesterone concentrations but positively associated with testosterone concentrations. Among CD8 TRM subsets, $CD69^{+}$ $CD103^{+}$ (DP) populations were significantly increased with high testosterone, whereas $CD69^{+}$ $CD103^{-}$ (SP) populations exhibited a similar, though nonsignificant, trend. Although this study did not evaluate longitudinal hormonal fluctuations, cycling donors exhibited the highest progesterone levels and the lowest ectocervical CD8 DP cell numbers (12-fold decrease). These observations suggest that dynamic hormonal changes under menstrual cycle regulation may reduce TRM durability. Consistent with these findings, comparing CD8 TRM gene expression profiles across testosterone states revealed differential enrichment of signaling pathways, particularly estrogen-response gene programs, despite comparable estrogen levels. This was accompanied by increased gene programs associated with immune function and cellular metabolism, but with decreased hypoxia and cell stress responses. These observations suggest that androgen-associated signaling contributes to differences in ectocervical CD8 TRM state and abundance; however, the cross-sectional design and heterogeneity in exogenous hormone exposure preclude attributing these differences specifically to testosterone in this study. Although understanding the specific influences of sex hormones on FRT TRM biology requires further investigation, various T cell immune functions are regulated through both estrogen and androgen receptor signaling[45-48]. Furthermore, because testosterone can antagonize estrogen-response signaling in hormone-responsive tissue[49,50], this raises the possibility that similar crosstalk contributed to the FRT CD8 TRM adaptations discovered in this investigation.

In conclusion, this study provides new insights into TRM biology across the female reproductive tract (FRT) and identifies sex hormones as important regulators of TRM.

These findings provide insights into the factors influencing TRM maintenance in the FRT and may help guide future studies aimed at improving immune protection against urogenital infections.

Materials and Methods:

Participants

This study protocol was approved by the Emory University School of Medicine Institutional Review Board (Approval number: 2024P008041); all donors provided informed consent. Eligibility criteria were that donors were adults (over 18 years), assigned female at birth, of reproductive age (less than 45 years), with negative current age-specific cervical cancer screening, and undergoing a routine minimally invasive hysterectomy procedure at Emory University Midtown Hospital. In addition to the medical eligibility criteria for minimally invasive hysterectomy based on the American College of Obstetricians and Gynecologists (ACOG) guidelines, participants were excluded if they had a recent genital tract infection, a recent pregnancy, abnormal uterine bleeding, or benign gynecologic lesions such as uterine fibroids or endometrial polyps. A pathologist evaluated extracted tissues for abnormalities that would preclude immune profiling, including incidental lesions, masses, or structural abnormalities. In some cases, cervical tissue was not provided if the cervix was not removed.

Tissue Processing

Hysterectomy tissues were separated into major sections by a pathologist prior to tissue transport. Each tissue type (uterus, endocervix, and ectocervix) was weighed (tissue weights from specimen ID #1 were not available), mechanically chopped, then enzymatically digested using Liberase TL (Thermolysin low): a blend of collagenase I/II [123μg/ml] and Thermolysin [7.5μg/ml] (Roche), DNase (50U/ml, Sigma-Aldrich), and Trypsin Inhibitor (1mg/ml, ThermoFisher). Tissue was digested at 37°C with constant shaking at 200rpm. Immediately following digestion, samples were passed through a 500μm mesh sieve and rinsed with complete RPMI 1640/L-glutamine (Gibco) supplemented with 10% heat-inactivated fetal bovine serum, penicillin/streptomycin (Corning), sodium pyruvate (Fisher Scientific), and non-essential amino acids (Gibco). Cell suspensions were then filtered through a 70μm sieve (Advantech) before being centrifuged at 400 x g for 10 minutes to pellet the cells. Mononuclear cells were isolated by Percoll density gradient centrifugation (GE Healthcare). Leukocyte fractions were collected, washed, and enumerated using a cell counter. Blood samples were collected into CPT tubes and centrifuged to separate the lymphocyte-enriched fraction from plasma. Cells were then washed in cell media. Blood plasma was aliquoted into cryovials and stored at -80°C. Isolated cells from hysterectomy tissues or blood were either used directly for cell analysis or cryopreserved in cryovials for RNA/TCR sequencing using

freezing media (90% HI-FBS, 10% DMSO). Cell cryovials were initially stored at -80°C in a controlled-rate freezing container for 24 hours and subsequently transferred to liquid nitrogen for long-term storage.

Flow Cytometry

Single-cell suspensions were stained for viability using Zombie NIR Fixable Viability Kits (BioLegend), followed by cell surface staining and measurements using a BD LSRFortessa (BD Biosciences) or Aurora spectral flow cytometer (Cytek Biosciences). These data were analyzed using FlowJo software (TreeStar, Inc.). CCR5 validations were performed from a donor subgroup (n=8). The following fluorochrome-conjugated antibodies were used:

ANTIBODY	*CONJUGATE*	*CLONE*	*VENDOR*
CD3	BUV737	SK7	BD Biosciences
CD4	BUV496	SK3	BD Biosciences
CD8	AF700	RPA-T8	Biolegend
CD11B	BV605	M1/70	Biolegend
CD16	BV711	3G8	Biolegend
CD56	PE	5.1H11	Biolegend
CD45	PE-Cy7	HI30	Biolegend
CD45RA	BV510	5H9	BD Biosciences
CD69	BUV395	FN50	BD Biosciences
CD103	APC	Ber-ACT8	Biolegend
CCR5	BV421	J418F1	Biolegend
CCR7	PE CF594	150503	BD Biosciences
HLA-DR	BV750	L243	Biolegend

Sex hormone measurement

Frozen blood plasma samples were transported on dry ice to the Emory University Biomarker Core Laboratory for sex hormone quantification in one batch run. Plasma concentrations of estradiol, testosterone, and progesterone were measured using validated liquid chromatography-tandem mass spectrometry (LC-MS/MS) assays. Assay services were provided by the Biomarkers Core Laboratory at the Emory National Primate Research Center. This facility is supported by the Emory National Primate Research Center Base Grant P51 OD011132

Statistics

Specific modeling approaches are described in the figure legends. Multiple comparisons were donor-matched. To explore potential associations between sex hormones and T cell phenotypes within distinct FRT regions for a small dataset, we used Spearman rank correlations with P-values < 0.05, which were validated independently or adjusted for multiple comparisons using the Benjamini–Hochberg false discovery rate (FDR) procedure. Statistical analyses of cell measurements were performed using GraphPad Prism version 10.2.2.

Single-cell RNA sequencing and analysis pipelines

Cryopreserved human leukocyte-enriched cells were gently thawed and stained prior to mechanical sorting for viability using 7-AAD (7-amino-actinomycin D) viability stain (Biolegend) and forward/side scatter characteristics on a Cytek Aurora CS (Cytek Biosciences) through the Emory Pediatrics Flow Core. Specimens were thawed, sorted, and sequenced in one batch. Single-cell RNA libraries were generated according to the 10x Genomics Chromium Single Cell 5′ Reagent Kits User Guide (v2 Chemistry Dual Index). Approximately 15,000 cells were loaded per sample for GEM generation and library preparation. Library quality control and sequencing were performed, and Illumina FASTQ files were processed and aligned to the GRCh38-2024-A reference transcriptome using Cell Ranger v8.0.0 (10x Genomics). Biological replicates were aggregated using the Cell Ranger *aggr* pipeline with default parameters and analyzed together in a single Seurat v5.3.0 object. Donor identity was retained in the cell metadata: libraries ending in -1 were assigned to Donor 1 and libraries ending in -2 to Donor 2. Thus, donors were pooled for the primary cell-level analyses but retained as biological replicates; subset and tissue DEG analyses were also repeated independently within each donor.

Cells were excluded if they contained >15% mitochondrial transcripts, <300 detected genes, or >10,000 detected genes. Gene expression counts were normalized using Seurat's NormalizeData function (default log-normalization) and variance-scaled using *ScaleData*. No Seurat integration, Harmony correction, or other batch correction was applied, and dimensional reduction was performed on the resulting non-batch-corrected expression space. Variable features were identified with FindVariableFeatures, followed by principal component analysis (PCA) using *RunPCA*. The top principal components that demonstrated a cumulative explained variance of 80% were used to construct the shared nearest-neighbor graph with *FindNeighbors*, followed by clustering using *FindClusters* (resolution = 0.25, algorithm = 3). Uniform manifold approximation and projection (UMAP) was performed using *RunUMAP* based on the top principal components used for the nearest-neighbor graph.

Differentially expressed genes (DEGs) were identified using Seurat's *FindAllMarkers* for cluster markers and *FindMarkers* for prespecified subset and tissue comparisons. The Wilcoxon rank-sum test was used, with a minimum expression fraction of 0.10 in at least one comparison group and an absolute log2 fold-change threshold of 0.25. Reported adjusted P values were Seurat's Bonferroni-adjusted values across the genes tested within each comparison; genes with adjusted $P < 0.05$ were considered statistically significant. Volcano plots used the more stringent display threshold of absolute log2 fold-change > 0.5 together with adjusted $P < 0.05$. Because the primary tests were performed at the cell level, cells were not treated as independent donor-level biological replicates; the two-donor sample size limits donor-level statistical inference. Pathway analysis was performed using Single Cell Pathway Analysis v1.6.1.

TCR sequencing and analysis pipelines

T cell receptor (TCR) libraries were generated and processed simultaneously with scRNA-seq using the V(D)J reference for TCR reconstruction. Gene expression matrices were analyzed using Seurat (v5.3.0). TCR sequences were analyzed using scirpy (v0.22.2) and scanpy (v1.11.4), which integrated clonotype assignments with the gene expression counts. For the Cell Ranger/scirpy analyses, a clonotype was represented by the Cell Ranger raw_clonotype_id. Clonal expansion and diversity analyses in R were restricted to high-confidence productive TRB contigs, and the TRB raw_clonotype_id was used as the clonotype identity. Clonotypes were considered shared between tissues only when the same TRB raw_clonotype_id was detected in both ectocervical and uterine cells within the same transcript-defined phenotype group; sharing was quantified by set intersection, Jaccard index, and overlap coefficient. The Python descriptive analysis additionally represented a cell's clonotype by the paired TCRα and TCRβ CDR3 amino-acid sequences when both chains were available, or by the available single-chain sequence otherwise. These definitions were kept distinct from the TRB raw_clonotype_id definition used for tissue-sharing statistics. Clonal expansion, diversity, V(D)J gene usage, and CDR3 sequence analyses were performed using scirpy. TCR clonotypes were annotated according to transcript-defined CD4 and CD8 T-cell identities. Major T cell subsets were annotated based on the expression of CD4, CD8A, and CD8B. CD8 T cells were defined by high expression of CD8A and/or CD8B with absence of CD4 expression, whereas CD4 T cells were defined by high CD4 expression with the absence of CD8A or CD8B expression. TRM, TMM, and TEM subsets were defined using the markers CD69, ITGAE, and CCR7, again classifying a cell with any transcripts as positive for each of the markers. TRM were either single positive (SP: $CD69^{+}$ $ITGAE^{-}$), or double positive (DP: $CD69^{+}$ $ITGAE^{+}$), and all CCR7-negative. TMM were CD4 T cells that were CCR7-positive. TEM cells were defined as $CCR7^{-}$ $CD69^{-}$ $ITGAE^{-}$.

Tables and Figures

	Estradiol (pg/mL)	*Testosterone (ng/mL)*	*Progesterone (ng/mL)*
1	39.02	11.00	0.05
2	12.92	0.16	0.08
3	41.21	6.34	0.04
4	18.21	7.41	0.10
5	150.39	0.47	9.06
6	182.20	7.27	0.05
7	69.67	5.12	0.10
8	71.64	0.06	4.86
9	65.72	8.30	0.04
10	46.07	14.65	0.11
11	21.46	0.10	0.30
12	24.23	0.20	0.07
13	4.63	0.25	0.13
14	55.14	9.04	0.06
15	49.14	0.72	1.86
16	51.43	4.38	0.16

Table 1. The levels of estradiol, testosterone, and progesterone in each donor. Participant-reported exogenous hormone use is indicated.

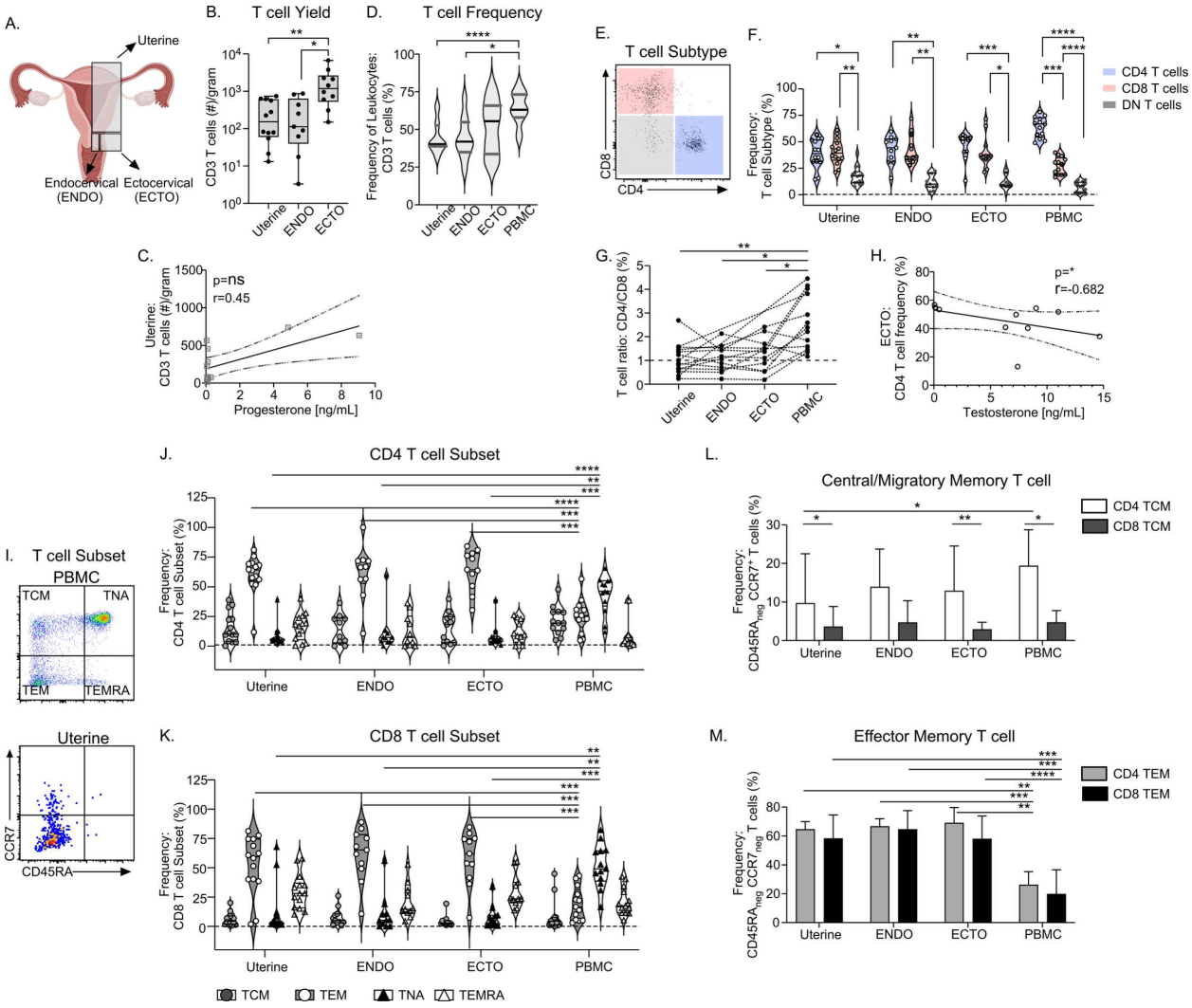
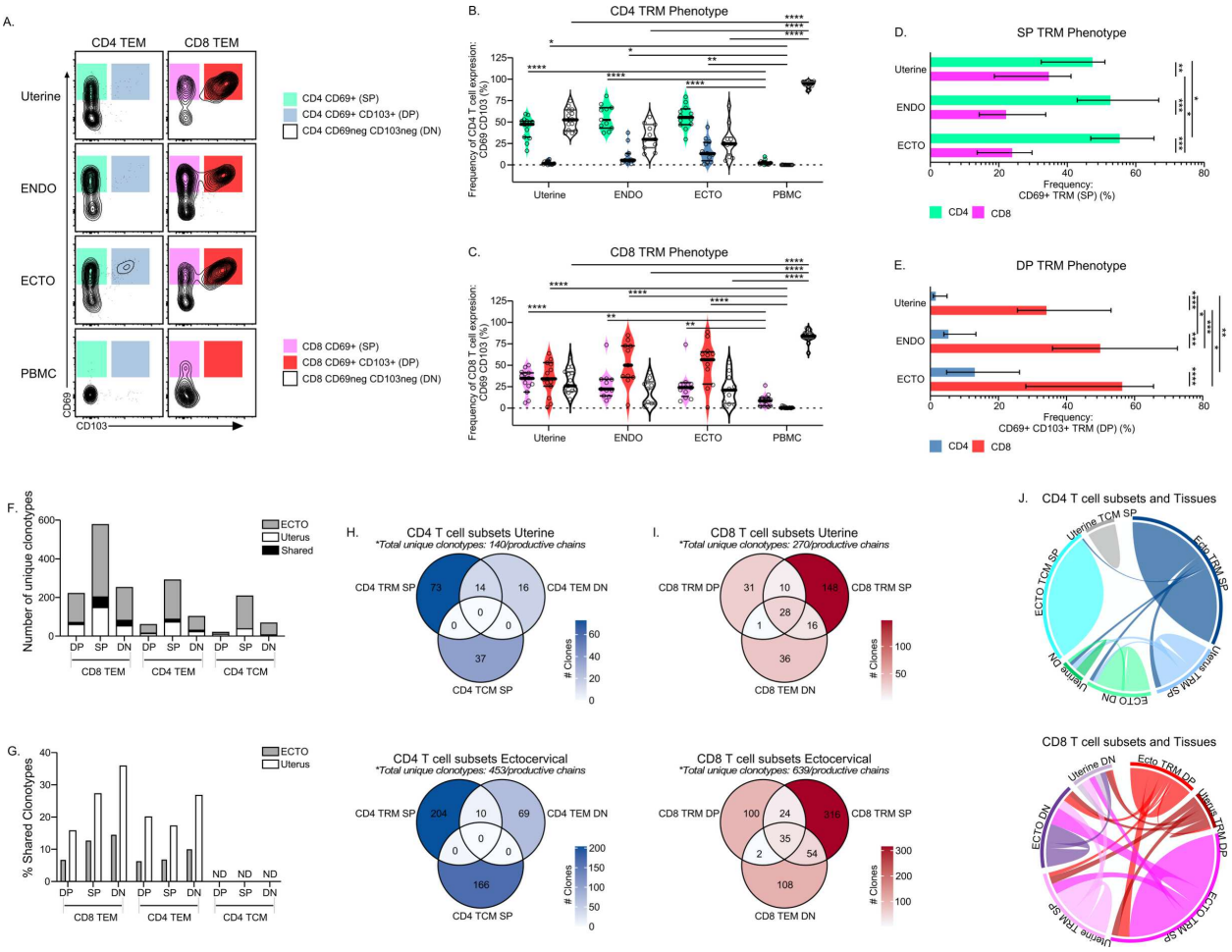


Figure 1. Memory T cell Distribution and Hormonal Associations within FRT Tissue Regions. (A). FRT cartoon illustrating key FRT tissue regions (highlighted in gray). Created with BioRender.com. (B). T cell yields per gram of available tissue from FRT regions. (C). Linear correlation between uterine T cell yields and progesterone measured from each donor. (D). T cell frequencies from the total leukocyte pool (viable CD45^{+} cells) in FRT regions and donor-matched PBMC. (E). Representative flow cytometry gating strategy used to identify T cell subtypes. (F). Frequency of CD4, CD8, and double-negative (DN) T cells across tissue regions. (G). Paired depiction of the T cell ratios. (H). Linear correlation between ectocervical CD4 T cell frequency and testosterone levels measured from each donor. (C, H). Correlations were assessed using a two-tailed Spearman correlation test; p-values and r/rho values are shown. (I). Representative pseudocolor flow cytometry plots of T cells from PBMC (top) and Uterine tissues (bottom), illustrating gating of CD4 and CD8 T cell subsets: Central memory T cells (TCM: CD45RA$_{neg}$ CCR7^{+}), Effector memory T cells (TEM: CD45RA$_{neg}$ CCR7$_{neg}$), Naïve T cells (TNA: CD45RA^{+} CCR7^{+}), and T effector memory RA (TEMRA: CD45RA^{+} CCR7$_{neg}$). (J,

K). Violin plot graph showing the frequency of CD4 (J) and CD8 (K) T cell memory subsets across FRT regions. (L). A direct comparison of CD4 T cell and CD8 TCM frequencies. (M). A direct comparison of CD4 T cell and CD8 TEM subset frequency. (L, M). Plotted as median with IQR. Statistical analysis for panels (B, D, F, G, J-M) was performed using a Mixed-effects analysis with Tukey's correction for multiple comparisons. Adjusted p-values are indicated (*p≤ 0.05, **p< 0.01, ***p< 0.001, ****p< 0.0001



587

588 **Figure 2. Resident T cell phenotypes and T cell receptor clonal sharing across the**
589 **FRT.** (A). Representative flow contour plots depicting TRM measurement from FRT
590 regions. Effector memory CD4 and CD8 T cells (TEM) were gated for CD69 and CD103
591 expression and identified as $CD69^{+}$ $CD103^{-}$ (single positive: SP), $CD69^{+}$ $CD103^{+}$ (double
592 positive: DP), or $CD69^{-}$ $CD103^{-}$ (double negative non-TRM: DN). (B). Frequencies of CD4
593 or (C). CD8 phenotypes across different tissue regions. (D). Comparative distribution of
594 SP and (E). DP phenotypes between CD4 and CD8 T cells, shown as median with
595 interquartile range (IQR). (B-E) Statistical analysis was performed using a Mixed-effects
596 analysis with Tukey's correction for multiple comparisons. Adjusted p-values are indicated
597 (*p≤0.05, **p<0.01, ***p<0.001, ****p<0.0001). (F). Number of unique and shared
598 clonotypes from T cell subsets in different FRT tissues. (G). Percentage of shared
599 clonotypes from T cell subsets. ND: not detected. (H) Venn diagrams showing unique and
600 shared clonotypes among CD4 (blue) and (I). CD8 (red) T cell subsets in uterine (top)
601 and ectocervical (bottom) tissues. (J) Circos plots illustrating clonotype sharing across
602 tissues in CD4 (top) or CD8 (bottom) T cell subsets.

603

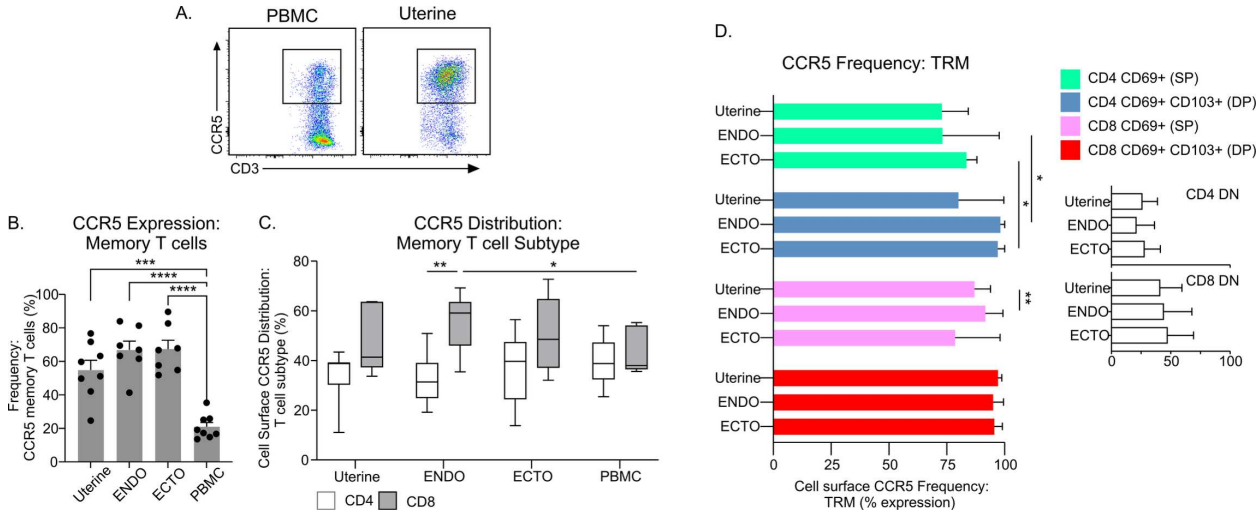


Figure 3. Cell surface CCR5 is enriched on TRM across the FRT. (A). Representative donor flow plots demonstrating cell surface CCR5 measurement from PBMC or uterine memory (CD45RA negative) T cells. (B). CCR5 frequency comparisons from PBMC or FRT TEM. (C). CCR5 distribution in T cell subtypes. (D). CCR5 frequencies from FRT compared by phenotype and FRT compartment (plotted as mean with SD). Non-TRM DN subsets are shown as insets. Statistical analysis for panels (B-E) was performed using a Mixed-effects analysis with Tukey's correction for multiple comparisons. Adjusted p-values are indicated (*p≤ 0.05, **p< 0.01, ***p< 0.001, ****p< 0.0001).

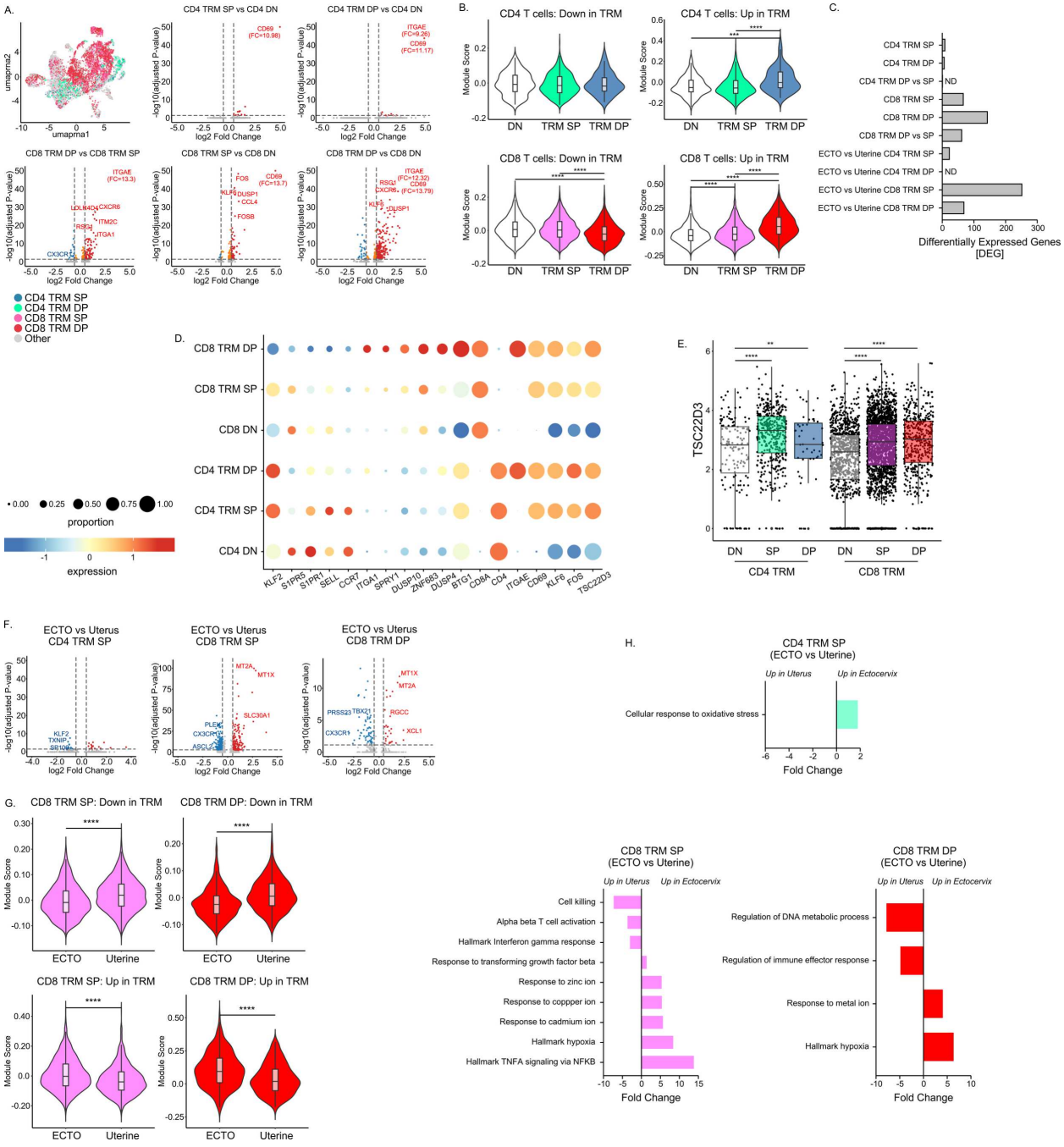
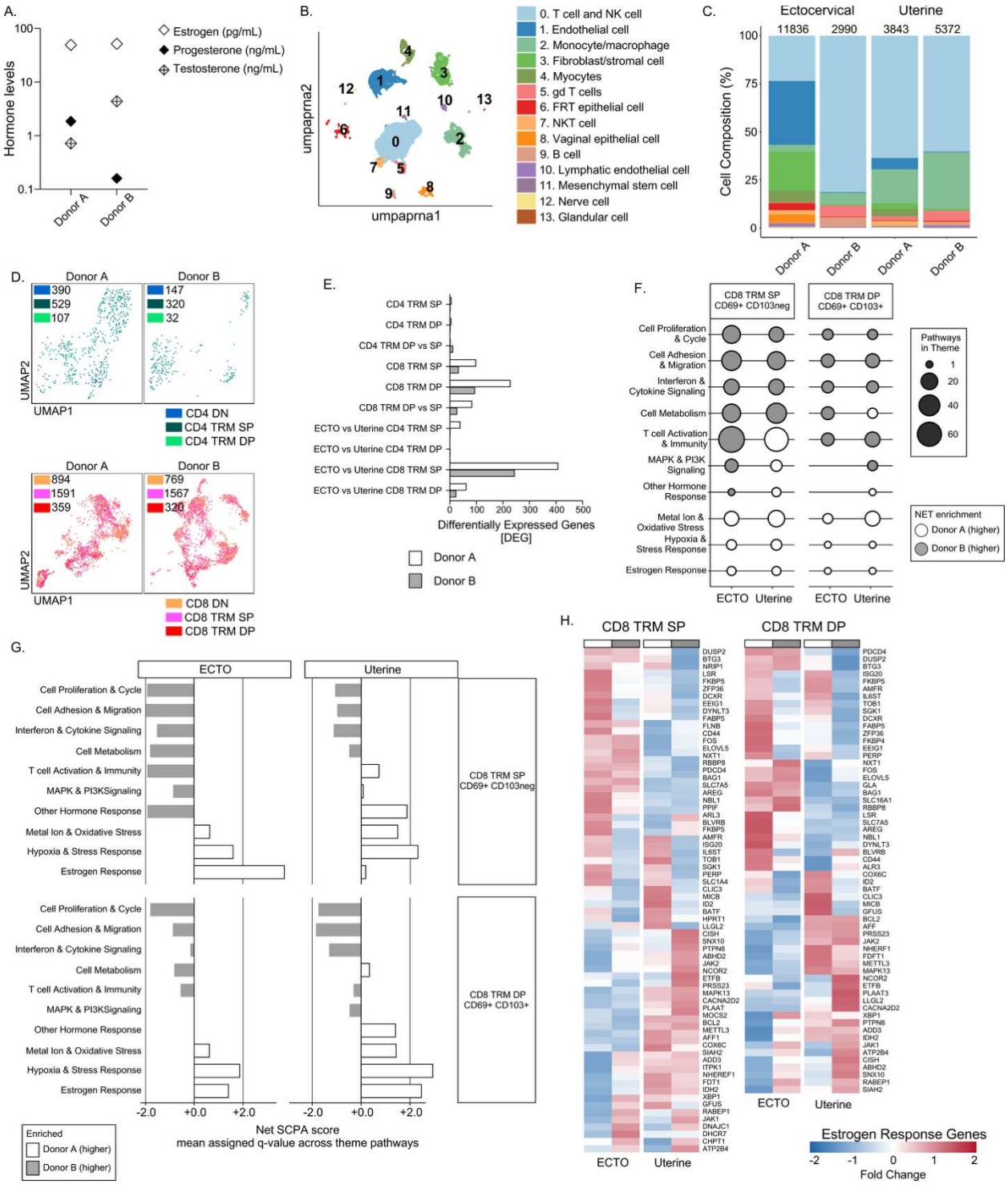


Figure 4. Transcriptional profiling identifies subtype and regional TRM heterogeneities. (A). UMAP emphasizing FRT TRM gene profiles with corresponding volcano plots of differentially expressed genes (DEGs) in subsets. (B). A comparison of CD4 and CD8 gene signatures using TRM module scores. (C). The number of TRM DEGs based on subtype and FRT region. (D). Bubble plot of TRM-associated genes expressed in subsets. (E). Individual TSC22D3 transcripts from subsets. (F). Volcano plots of CD4 SP and CD8 TRM subset DEGs compared by region. (G). Gene signatures from CD8 subsets compared by region using TRM module scores. (H). Fold change in gene

pathways from TRM, compared by region. Significant changes across donors are shown. (B, E, G) Statistical analysis of mean comparisons was performed using a two-way ANOVA. P-values are indicated (*p≤ 0.05, **p< 0.01, ***p< 0.001, ****p< 0.0001, ND: not detected).



641

642 **Figure 5. FRT TRM transcriptional programming distinguished by hormone status.**
643 (A). Hormone levels compared by donor. (B). UMAP clustering and identification of viable
644 sorted FRT cells. (C). The percent of cell types identified in the ectocervical or uterine
645 tissues stratified by individual donors, with the total cell number per tissue indicated. (D).
646 UMAPs comparing CD4 and CD8 TRM genes from each donor. (E). The number of DEGs

based on subtype and FRT region from individual donors. (F). Bubble plots comparing SP or DP CD8 gene pathway themes by donor and tissue. (G). Bar plots showing gene pathway themes by single-cell pathway analysis (SCPA) score, stratified by donor and tissue. (H). Heat map measuring the fold change in hallmark estrogen response genes in CD8 DP compared by donor and FRT compartment.

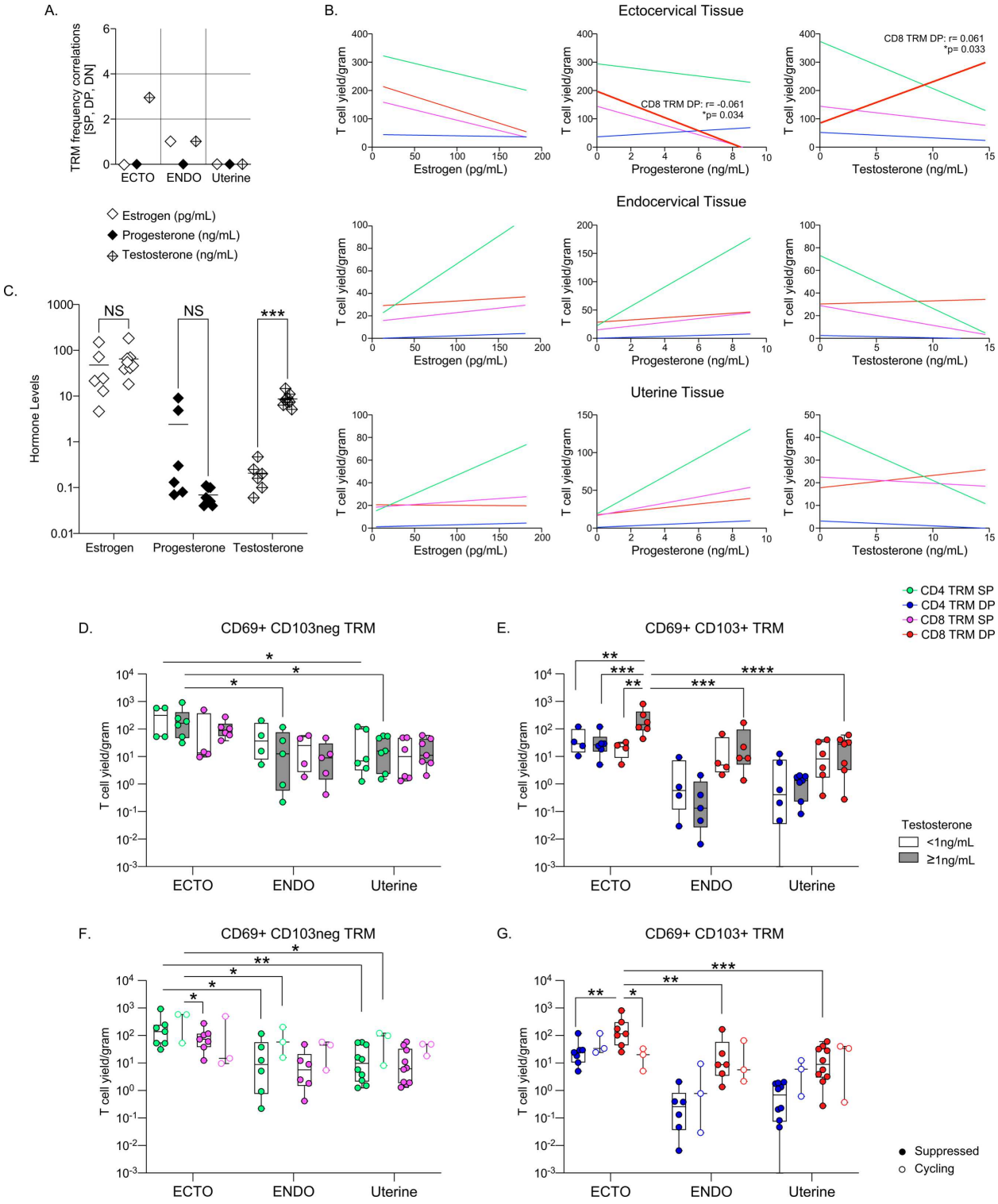


Figure 6. Sex hormone associations with cervical T cell composition and abundance. (A). The number of significant correlations between T cell phenotype frequency (DN, SP, DP) in distinct FRT regions and sex-hormone levels. (B). Correlations between total yield (per gram of tissue) of SP or DP TRM and hormone levels from

cervical and uterine tissues. Association trends were assessed using Spearman rank correlations; |rho| values ≤ 0.4 were further evaluated for directionality using a one-tailed analysis; p-values< 0.05 are shown. (C). Sex-hormone levels stratified by high and low testosterone in Donors. (D). Direct measurement of SP and (E). DP total cell yields stratified by low or high donor testosterone levels. (F). A comparison of SP and (G). DP TRM cell yields stratified by reported cycling status. (C-F). Statistical analysis was performed using a Mixed-effects analysis with Tukey's correction for multiple comparisons. Adjusted p-values are indicated (*p≤ 0.05, **p< 0.01, ***p< 0.001, ****p< 0.0001, or NS: not significant).

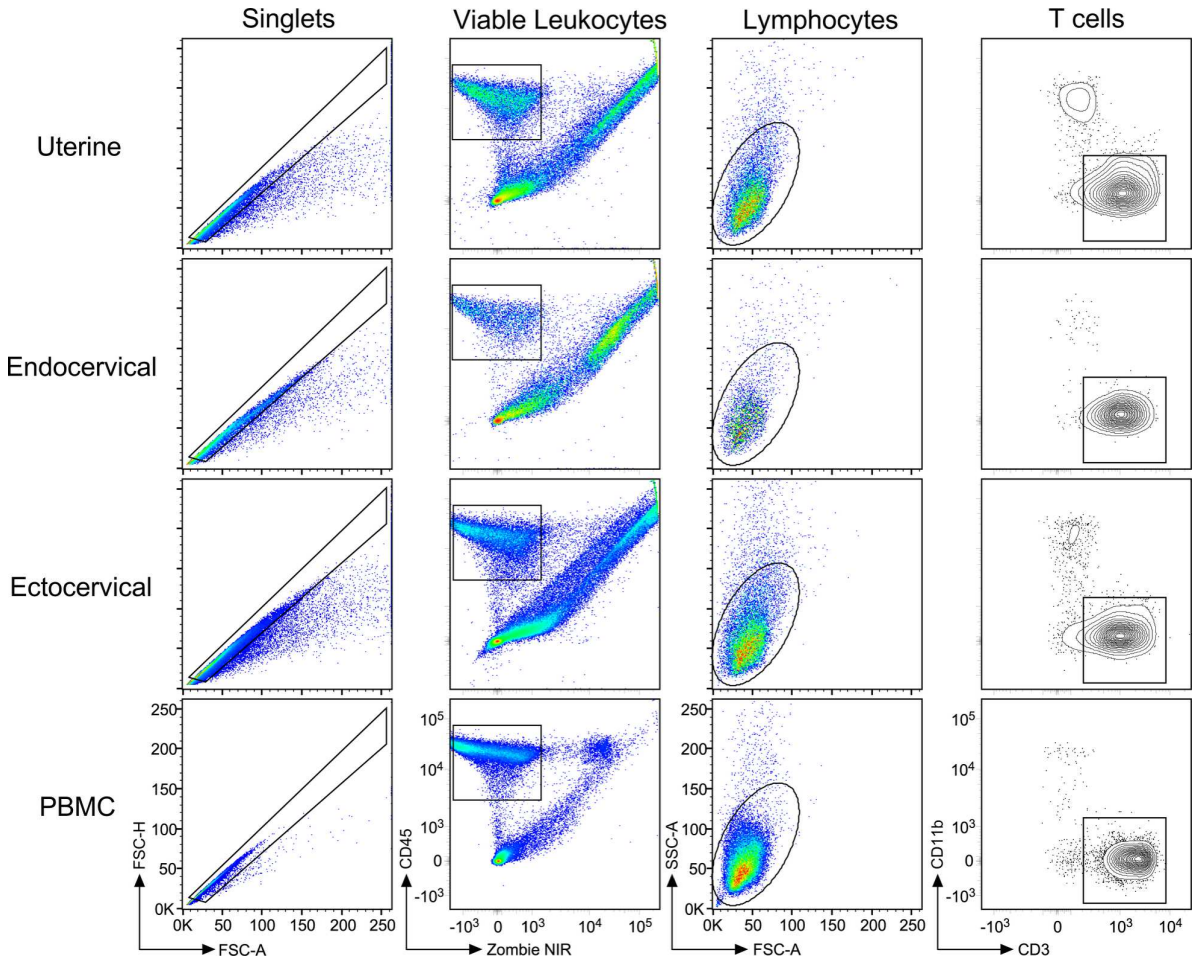
Supplemental Data:

ID	*Topical Testosterone*	*Injectable Testosterone*	*Oral Progesterone*	*Oral Estradiol*	*Cycling*	*Estradiol (pg/mL)*	*Testosterone (ng/mL)*	*Progesterone (ng/mL)*
1		Y				39.02	11.00	0.05
2	Y		Y			12.92	0.16	0.08
3		Y				41.21	6.34	0.04
4		Y				18.21	7.41	0.10
5	Y	Y			Y	150.39	0.47	9.06
6		Y				182.20	7.27	0.05
7		Y				69.67	5.12	0.10
8					Y	71.64	0.06	4.86
9		Y				65.72	8.30	0.04
10		Y				46.07	14.65	0.11
11					Y	21.46	0.10	0.30
12			Y			24.23	0.20	0.07
13			Y	Y		4.63	0.25	0.13
14		Y				55.14	9.04	0.06
15	Y				Y	49.14	0.72	1.86
16		Y				51.43	4.38	0.16
Total	3	10	3	1	4			

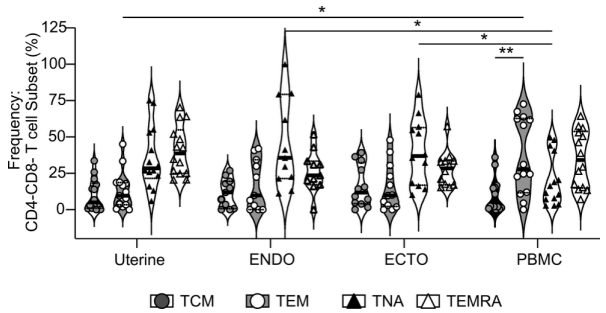
S. Table 1. Reported hormone and cycling status by donors indicated by Y (yes) compared with circulating sex hormone measurements.

	ECTO CD4 TCM	SP	DP	DN	ECTO CD4 TEM	SP	DP	DN	ECTO CD8 TEM	SP	DP	DN
Estradiol versus												
Spearman r		-0.1727	0.1240	0.1182		-0.6000	-0.2545	0.7273		0.1182	-0.3273	0.5818
P value (two-tailed)		0.6146	0.7200	0.7346		0.0562	0.4510	0.0144		0.7346	0.3268	0.0656
BH-FDR q		0.7346	0.7346	0.7346		0.1686	0.7346	0.0864		0.7346	0.4902	0.1968
P value summary		ns	ns	ns		ns	ns	ns		ns	ns	ns
Progesterone versus												
Spearman r		0.2648	0.4789	-0.3333		0.1050	0.5160	-0.4749		0.2648	0.0776	-0.2831
P value (two-tailed)		0.4280	0.1374	0.3138		0.7586	0.1072	0.1416		0.4280	0.8218	0.3958
BH-FDR q		0.5136	0.2832	0.4708		0.7586	0.2832	0.2832		0.6420	0.8218	0.6420
P value summary		ns	ns	ns		ns	ns	ns		ns	ns	ns
Testosterone versus												
Spearman r		-0.7455	-0.7532	0.8000		-0.4545	0.1364	0.3545		-0.5727	0.0182	0.4273
P value (two-tailed)		0.0112	0.0112	0.0046		0.1634	0.6938	0.2862		0.0708	0.9674	0.1928
BH-FDR q		**0.0224**	**0.0224**	**0.0224**		0.2452	0.6938	0.3434		0.2124	0.9674	0.2892
P value summary		**YES**	**YES**	**YES**		ns	ns	ns		ns	ns	ns
	ENDO CD4 TCM	**SP**	**DP**	**DN**	**ENDO CD4 TEM**	**SP**	**DP**	**DN**	**ENDO CD8 TEM**	**SP**	**DP**	**DN**
Estradiol versus												
Spearman r		0.3587	0.3073	-0.3587		-0.2606	-0.1515	0.3212		0.2121	-0.4909	0.7697
P value (two-tailed)		0.3060	0.3826	0.3060		0.4698	0.6820	0.3678		0.5602	0.1548	0.0126
BH-FDR q		0.5638	0.5638	0.5638		0.5638	0.6820	0.5638		0.5602	0.2322	**0.0378**
P value summary		ns	ns	ns		ns	ns	ns		ns	ns	**YES**
Progesterone versus												
Spearman r		0.0765	0.4362	-0.0765		0.1463	0.3171	-0.4024		0.5427	-0.4817	0.0366
P value (two-tailed)		0.8332	0.2084	0.8332		0.6854	0.3688	0.2480		0.1092	0.1608	0.9246
BH-FDR q		0.8332	0.7376	0.8332		0.8332	0.7376	0.7376		0.2412	0.2520	0.9246
P value summary		ns	ns	ns		ns	ns	ns		ns	ns	ns
Testosterone versus												
Spearman r		-0.0547	-0.6145	0.0547		-0.6000	0.2485	0.0546		-0.8303	0.5152	0.3333
P value (two-tailed)		0.8840	0.0624	0.8840		0.0734	0.4918	0.8916		0.0048	0.1334	0.3488
BH-FDR q		0.8916	0.2202	0.8916		0.2202	0.8916	0.8916		**0.0144**	0.2002	0.3488
P value summary		ns	ns	ns		ns	ns	ns		**YES**	ns	ns
	Uterine CD4 TCM	**SP**	**DP**	**DN**	**Uterine CD4 TEM**	**SP**	**DP**	**DN**	**Uterine CD8 TEM**	**SP**	**DP**	**DN**
Estradiol versus												
Spearman r		-0.0330	0.5562	-0.4026		0.1121	0.3187	-0.1560		0.1824	-0.4857	0.4066
P value (two-tailed)		0.9122	0.0424	0.1536		0.7042	0.2666	0.5944		0.5322	0.0810	0.1506
BH-FDR q		0.9122	0.2544	0.4608		0.8450	0.5332	0.8450		0.5322	0.2260	0.2260
P value summary		ns	ns	ns		ns	ns	ns		ns	ns	ns
Progesterone versus												
Spearman r		0.5751	0.0777	-0.3322		0.5006	0.4520	-0.5072		0.4013	-0.1522	0.0265
P value (two-tailed)		0.0338	0.7906	0.2434		0.0704	0.1060	0.0664		0.1550	0.6010	0.9304
BH-FDR q		0.1408	0.7906	0.2920		0.1408	0.1590	0.1408		0.4650	0.9016	0.9304
P value summary		ns	ns	ns		ns	ns	ns		ns	ns	ns
Testosterone versus												
Spearman r		-0.6271	-0.2370	0.5391		-0.2835	0.1121	0.1473		-0.4374	0.0286	0.0198
P value (two-tailed)		0.0186	0.4126	0.0492		0.3254	0.7042	0.6158		0.1198	0.9276	0.9516
BH-FDR q		0.1116	0.6190	0.1476		0.6190	0.7042	0.7042		0.3594	0.9516	0.9516
P value summary		ns	ns	ns		ns	ns	ns		ns	ns	ns

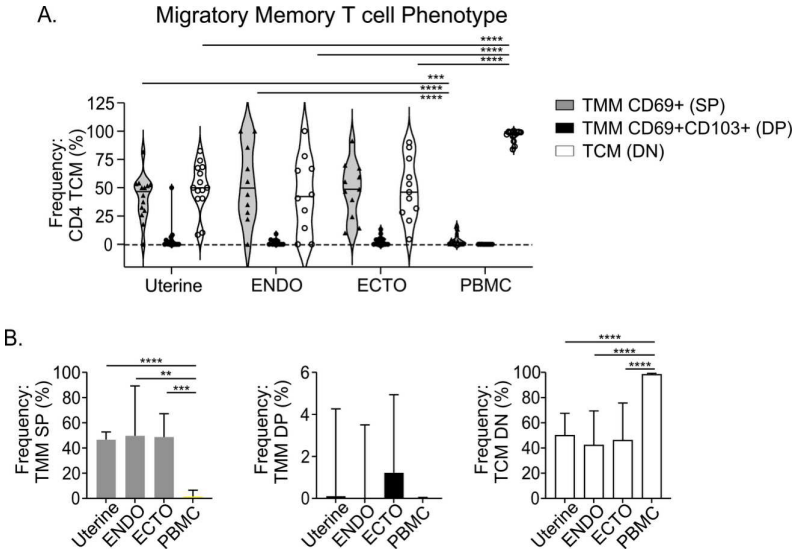
S Table 2. Associations between sex hormone concentrations, TMM phenotypes, and T-cell lineage TRM phenotypes at individual tissue sites were tested for significance using Spearman rank correlation. To account for multiple testing, results were adjusted using the Benjamini–Hochberg (BH) false discovery rate (FDR) procedure within prespecified tissue-, TRM lineage-, and hormone-specific families of phenotypic comparisons. An FDR-adjusted q value< 0.05 was considered statistically significant, ns-not significant.



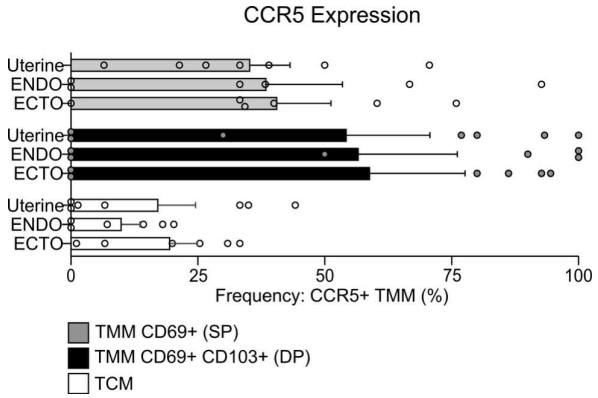
S Figure 1: The flow gating strategy for measuring T cells from suspension. From left to right, singlet cells are gated for immune cells and viability. Cells are then measured for lymphocytes by size and granularity characteristics. T cells ($CD3^+$ lymphocytes) are discriminated from NK cells (CD16, CD56 expression) and myeloid cells (shown as CD11b expression) prior to characterization. Matched-PBMC gating was applied to FRT cells for measurements.



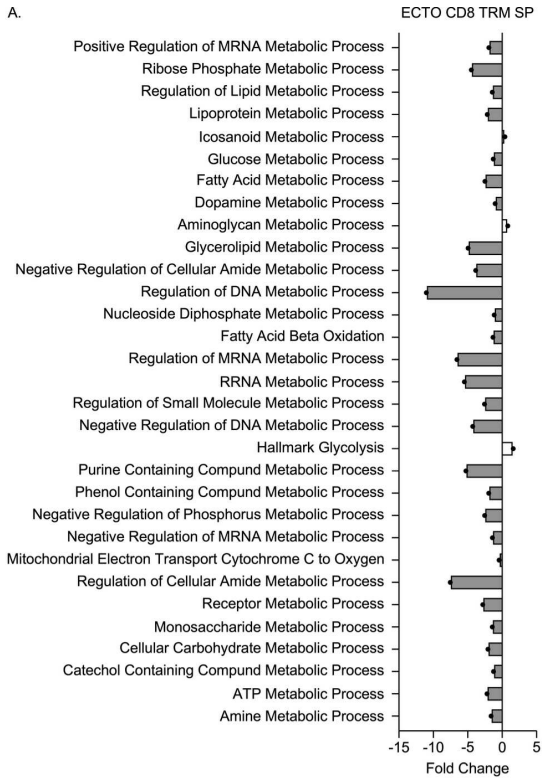
S Figure 2: Violin plot graph showing the frequency of CD4- CD8- T cell memory subsets across FRT regions. Statistical analysis was performed using a Mixed-effects analysis with Tukey's correction for multiple comparisons. Adjusted p-values are indicated (*p≤0.05, **p<0.01, ***p<0.001, ****p<0.0001).

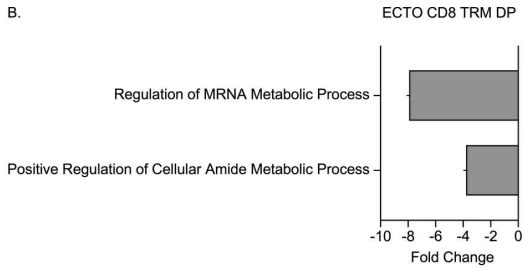


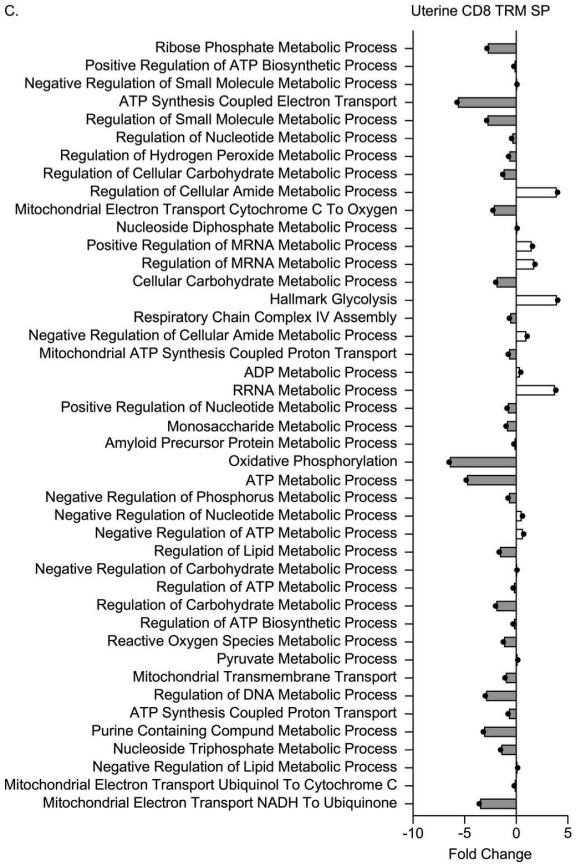
S Figure 3: (A). CD4 TMM phenotypes across different tissue regions. (B). Direct comparison of TMM subsets or TCM, plotted as the median value with interquartile range (IQR). Statistical analysis was performed using a Mixed-effects analysis with Tukey's correction for multiple comparisons. Adjusted p-values are indicated (*p≤0.05, **p<0.01, ***p<0.001, ****p<0.0001).

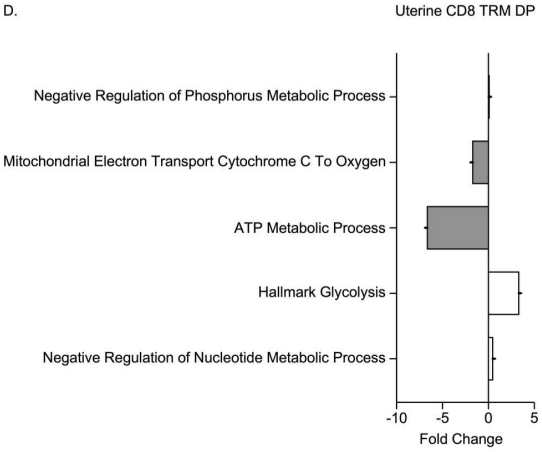


S Figure 4: CCR5 frequencies from TMM subsets and TCM populations. Statistical analysis was performed using a Mixed-effects analysis with Tukey's correction for multiple comparisons. No comparisons were significant.


A.
ECTO CD8 TRM SP
Positive Regulation of MRNA Metabolic Process
Ribose Phosphate Metabolic Process
Regulation of Lipid Metabolic Process
Lipoprotein Metabolic Process
Icosanoid Metabolic Process
Glucose Metabolic Process
Fatty Acid Metabolic Process
Dopamine Metabolic Process
Aminoglycan Metabolic Process
Glycerolipid Metabolic Process
Negative Regulation of Cellular Amide Metabolic Process
Regulation of DNA Metabolic Process
Nucleoside Diphosphate Metabolic Process
Fatty Acid Beta Oxidation
Regulation of MRNA Metabolic Process
RRNA Metabolic Process
Regulation of Small Molecule Metabolic Process
Negative Regulation of DNA Metabolic Process
Hallmark Glycolysis
Purine Containing Compund Metabolic Process
Phenol Containing Compund Metabolic Process
Negative Regulation of Phosphorus Metabolic Process
Negative Regulation of MRNA Metabolic Process
Mitochondrial Electron Transport Cytochrome C to Oxygen
Regulation of Cellular Amide Metabolic Process
Receptor Metabolic Process
Monosaccharide Metabolic Process
Cellular Carbohydrate Metabolic Process
Catechol Containing Compund Metabolic Process
ATP Metabolic Process
Amine Metabolic Process
-15 -10 -5 0 5
Fold Change


B.
ECTO CD8 TRM DP
Regulation of MRNA Metabolic Process
Positive Regulation of Cellular Amide Metabolic Process
-10 -8 -6 -4 -2 0
Fold Change


C.
Uterine CD8 TRM SP
Ribose Phosphate Metabolic Process
Positive Regulation of ATP Biosynthetic Process
Negative Regulation of Small Molecule Metabolic Process
ATP Synthesis Coupled Electron Transport
Regulation of Small Molecule Metabolic Process
Regulation of Nucleotide Metabolic Process
Regulation of Hydrogen Peroxide Metabolic Process
Regulation of Cellular Carbohydrate Metabolic Process
Regulation of Cellular Amide Metabolic Process
Mitochondrial Electron Transport Cytochrome C To Oxygen
Nucleoside Diphosphate Metabolic Process
Positive Regulation of MRNA Metabolic Process
Regulation of MRNA Metabolic Process
Cellular Carbohydrate Metabolic Process
Hallmark Glycolysis
Respiratory Chain Complex IV Assembly
Negative Regulation of Cellular Amide Metabolic Process
Mitochondrial ATP Synthesis Coupled Proton Transport
ADP Metabolic Process
RRNA Metabolic Process
Positive Regulation of Nucleotide Metabolic Process
Monosaccharide Metabolic Process
Amyloid Precursor Protein Metabolic Process
Oxidative Phosphorylation
ATP Metabolic Process
Negative Regulation of Phosphorus Metabolic Process
Negative Regulation of Nucleotide Metabolic Process
Negative Regulation of ATP Metabolic Process
Regulation of Lipid Metabolic Process
Negative Regulation of Carbohydrate Metabolic Process
Regulation of ATP Metabolic Process
Regulation of Carbohydrate Metabolic Process
Regulation of ATP Biosynthetic Process
Reactive Oxygen Species Metabolic Process
Pyruvate Metabolic Process
Mitochondrial Transmembrane Transport
Regulation of DNA Metabolic Process
ATP Synthesis Coupled Proton Transport
Purine Containing Compund Metabolic Process
Nucleoside Triphosphate Metabolic Process
Negative Regulation of Lipid Metabolic Process
Mitochondrial Electron Transport Ubiquinol To Cytochrome C
Mitochondrial Electron Transport NADH To Ubiquinone
-10 -5 0 5
Fold Change


D.
Uterine CD8 TRM DP
Negative Regulation of Phosphorus Metabolic Process
Mitochondrial Electron Transport Cytochrome C To Oxygen
ATP Metabolic Process
Hallmark Glycolysis
Negative Regulation of Nucleotide Metabolic Process
-10 -5 0 5
Fold Change

821

S Figure 5: Fold change in metabolic gene pathways from (A, B) ectocervical and (C, D) uterine TRM, compared by region and SP (A, C) and DP (C, D) TRM subsets. Significant changes across donors are shown. Increases in Donor A are shown as white bars on the right axis, and increases in Donor B are shown as grey bars on the left axis.

Acknowledgments: We sincerely thank the study participants for their generous tissue donations, which made this research possible. At the Emory Biomarkers Core Laboratory, we thank Lori L. Fralick and Dr. Kelly Ethun for their assistance. We thank Sofia Rose Cendoya and Jina Li for assistance with tissue processing. We thank Dr. Paul Thomas for insights into TCR sequencing. We thank the Emory University School of Medicine Flow Cytometry Core (EFCC) Facility and Dr. Igor Albizua-Santin for assistance in mechanical cell sorting. This work was supported in part by the Georgia Clinical & Translational Science Alliance of the National Institutes of Health under Award Number UL1TR002378.

Funding: R21AI180610 (ASK), 1R01HD116985-01A1 (ASK)

Data Availability Declaration: The single-cell RNA sequencing and T-cell receptor sequencing data generated in this study will be deposited in the NCBI Gene Expression Omnibus (GEO) or an appropriate controlled-access repository and made available upon publication. All data supporting the findings of this study, including flow cytometry measurements, sex hormone concentrations, and statistical analyses, will be provided in the manuscript, Supplementary Information, and accompanying Source Data files. Individual-level human donor data that could compromise participant confidentiality will not be made publicly available. Additional de-identified data may be obtained from the corresponding author upon reasonable request, subject to institutional and ethical approvals.

Author Contribution Declaration: A.S.K. and J.E.K. conceived and designed the study. E.M.B.C., R.S.V., M.E.W., P.V., S.L.H., K.J.H., and C.L.R.M. contributed to experimental investigations and data collection. C.D.S. contributed to transcriptomic analysis and interpretation. E.J.P. and T.D. provided scientific expertise and contributed to the interpretation of findings. E.M.B.C., R.S.V., M.E.W., and A.S.K. analyzed and interpreted the data. E.M.B.C., R.S.V., and A.S.K. drafted the manuscript. All authors reviewed and edited the manuscript and approved the final version.

References

1 Gebhardt, T. *et al.* Memory T cells in nonlymphoid tissue that provide enhanced local immunity during infection with herpes simplex virus. *Nat Immunol* **10**, 524-530 (2009). https://doi.org/10.1038/ni.1718

2 Sheridan, B. S. *et al.* Oral infection drives a distinct population of intestinal resident memory CD8(+) T cells with enhanced protective function. *Immunity* **40**, 747-757 (2014). https://doi.org/10.1016/j.immuni.2014.03.007

3 Uddbäck, I. *et al.* Prevention of respiratory virus transmission by resident memory CD8. *Nature* (2023). https://doi.org/10.1038/s41586-023-06937-1

4 Stary, G. *et al.* VACCINES. A mucosal vaccine against Chlamydia trachomatis generates two waves of protective memory T cells. *Science* **348**, aaa8205 (2015). https://doi.org/10.1126/science.aaa8205

5 Szabo, P. A., Miron, M. & Farber, D. L. Location, location, location: Tissue resident memory T cells in mice and humans. *Sci Immunol* **4** (2019). https://doi.org/10.1126/sciimmunol.aas9673

6 Peng, T. *et al.* Tissue-Resident-Memory CD8. *Front Immunol* **12**, 735643 (2021). https://doi.org/10.3389/fimmu.2021.735643

7 Li, J., Xiao, C., Li, C. & He, J. Tissue-resident immune cells: from defining characteristics to roles in diseases. *Signal Transduct Target Ther* **10**, 12 (2025). https://doi.org/10.1038/s41392-024-02050-5

8 Postat, J. *et al.* Mechanosensing by T cells promotes a tissue-resident memory transcriptional program. *Nat Immunol* **27**, 1708-1721 (2026). https://doi.org/10.1038/s41590-026-02581-9

9 Poon, M. M. L. *et al.* Tissue adaptation and clonal segregation of human memory T cells in barrier sites. *Nat Immunol* **24**, 309-319 (2023). https://doi.org/10.1038/s41590-022-01395-9

10 Szabo, P. A. Axes of heterogeneity in human tissue-resident memory T cells. *Immunol Rev* **316**, 23-37 (2023). https://doi.org/10.1111/imr.13210

11 Snyder, M. E. *et al.* Modulation of tissue resident memory T cells by glucocorticoids after acute cellular rejection in lung transplantation. *J Exp Med* **219** (2022). https://doi.org/10.1084/jem.20212059

12 Hapgood, J. P., Kaushic, C. & Hel, Z. Hormonal Contraception and HIV-1 Acquisition: Biological Mechanisms. *Endocr Rev* **39**, 36-78 (2018). https://doi.org/10.1210/er.2017-00103

13 Wira, C. R., Rodriguez-Garcia, M. & Patel, M. V. The role of sex hormones in immune protection of the female reproductive tract. *Nat Rev Immunol* **15**, 217-230 (2015). https://doi.org/10.1038/nri3819

14 Kadel, S. *et al.* Androgens protect ILC2S from functional suppression during influenza virus infection. *Mucosal Immunol* **19**, 100337 (2026). https://doi.org/10.1016/j.mucimm.2026.03.011

15 Trumble, B. C. *et al.* Associations between male testosterone and immune function in a pathogenically stressed forager-horticultural population. *Am J Phys Anthropol* **161**, 494-505 (2016). https://doi.org/10.1002/ajpa.23054
16 Lakshmikanth, T. *et al.* Immune system adaptation during gender-affirming testosterone treatment. *Nature* **633**, 155-164 (2024). https://doi.org/10.1038/s41586-024-07789-z
17 Rodriguez-Garcia, M., Connors, K. & Ghosh, M. HIV Pathogenesis in the Human Female Reproductive Tract. *Curr HIV/AIDS Rep* **18**, 139-156 (2021). https://doi.org/10.1007/s11904-021-00546-1
18 Yüzen, D., Arck, P. C. & Thiele, K. Tissue-resident immunity in the female and male reproductive tract. *Semin Immunopathol* **44**, 785-799 (2022). https://doi.org/10.1007/s00281-022-00934-8
19 Elliott Williams, M. *et al.* The menstrual cycle regulates migratory CD4 T-cell surveillance in the female reproductive tract via CCR5 signaling. *Mucosal Immunol* (2023). https://doi.org/10.1016/j.mucimm.2023.10.002
20 Swaims-Kohlmeier, A. *et al.* Progesterone Levels Associate with a Novel Population of CCR5+CD38+ CD4 T Cells Resident in the Genital Mucosa with Lymphoid Trafficking Potential. *J Immunol* **197**, 368-376 (2016). https://doi.org/10.4049/jimmunol.1502628
21 Zheng, M. Z. M. & Wakim, L. M. Tissue resident memory T cells in the respiratory tract. *Mucosal Immunol* **15**, 379-388 (2022). https://doi.org/10.1038/s41385-021-00461-z
22 Woodland, D. L. & Kohlmeier, J. E. Migration, maintenance and recall of memory T cells in peripheral tissues. *Nat Rev Immunol* **9**, 153-161 (2009). https://doi.org/10.1038/nri2496
23 Sheridan, B. S. & Lefrancois, L. Regional and mucosal memory T cells. *Nat Immunol* **12**, 485-491 (2011).
24 Kumar, B. V. *et al.* Human Tissue-Resident Memory T Cells Are Defined by Core Transcriptional and Functional Signatures in Lymphoid and Mucosal Sites. *Cell Rep* **20**, 2921-2934 (2017). https://doi.org/10.1016/j.celrep.2017.08.078
25 Woodward Davis, A. S. *et al.* The human memory T cell compartment changes across tissues of the female reproductive tract. *Mucosal Immunol* **14**, 862-872 (2021). https://doi.org/10.1038/s41385-021-00406-6
26 Smith, N. P. *et al.* Resident memory T cell development is gradual and shows AP-1 gene expression in mature cells. *JCI Insight* **10** (2025). https://doi.org/10.1172/jci.insight.187381
27 Ayroldi, E. *et al.* Modulation of T-cell activation by the glucocorticoid-induced leucine zipper factor via inhibition of nuclear factor kappaB. *Blood* **98**, 743-753 (2001). https://doi.org/10.1182/blood.v98.3.743
28 Bereshchenko, O., Migliorati, G., Bruscoli, S. & Riccardi, C. Glucocorticoid-Induced Leucine Zipper: A Novel Anti-inflammatory Molecule. *Front Pharmacol* **10**, 308 (2019). https://doi.org/10.3389/fphar.2019.00308
29 Scott, M. C. *et al.* Deep profiling deconstructs features associated with memory CD8. *Immunity* **58**, 162-181.e110 (2025). https://doi.org/10.1016/j.immuni.2024.11.007
30 Choi, E. H. & Park, S. J. TXNIP: A key protein in the cellular stress response pathway and a potential therapeutic target. *Exp Mol Med* **55**, 1348-1356 (2023). https://doi.org/10.1038/s12276-023-01019-8

31 Montgomery, S. & Ingalls, R. R. Epithelial Changes in the Testosterone-Dominant Vagina: Implications for Menopause, Transgender Care, and Beyond. *Cells* **15** (2026). https://doi.org/10.3390/cells15090745

32 Baldassarre, M. *et al.* Effects of long-term high dose testosterone administration on vaginal epithelium structure and estrogen receptor-α and -β expression of young women. *Int J Impot Res* **25**, 172-177 (2013). https://doi.org/10.1038/ijir.2013.9

33 Poston, T. B. *et al.* Intranasal immunization with CPAF combined with ADU-S100 induces an effector CD4 T cell response and reduces bacterial burden following intravaginal infection with Chlamydia muridarum. *Vaccine* **43**, 126526 (2025). https://doi.org/10.1016/j.vaccine.2024.126526

34 Yount, K. S. & Darville, T. Immunity to Sexually Transmitted Bacterial Infections of the Female Genital Tract: Toward Effective Vaccines. *Vaccines (Basel)* **12** (2024). https://doi.org/10.3390/vaccines12080863

35 Corrado, M. & Pearce, E. L. Targeting memory T cell metabolism to improve immunity. *J Clin Invest* **132** (2022). https://doi.org/10.1172/JCI148546

36 Liu, G., Wang, Z. & Li, S. Heterogeneity and plasticity of tissue-resident memory T cells in skin diseases and homeostasis: a review. *Front Immunol* **15**, 1378359 (2024). https://doi.org/10.3389/fimmu.2024.1378359

37 de Almeida, G. P. *et al.* Human skin-resident host T cells can persist long term after allogeneic stem cell transplantation and maintain recirculation potential. *Sci Immunol* **7**, eabe2634 (2022). https://doi.org/10.1126/sciimmunol.abe2634

38 Klicznik, M. M. *et al.* Human CD4. *Sci Immunol* **4** (2019). https://doi.org/10.1126/sciimmunol.aav8995

39 O'Neil, T. R. *et al.* The Role of Tissue Resident Memory CD4 T Cells in Herpes Simplex Viral and HIV Infection. *Viruses* **13** (2021). https://doi.org/10.3390/v13030359

40 Swaims-Kohlmeier, A. *et al.* Proinflammatory oscillations over the menstrual cycle drives bystander CD4 T cell recruitment and SHIV susceptibility from vaginal challenge. *EBioMedicine* **69**, 103472 (2021). https://doi.org/10.1016/j.ebiom.2021.103472

41 Swaims-Kohlmeier, A. *et al.* CCR5 blockade inhibits menstrual-driven proinflammatory T cell infiltration into the cervicovaginal mucosa of women. *Sci Adv* **12**, eaed0347 (2026). https://doi.org/10.1126/sciadv.aed0347

42 Shacklett, B. L., Ouattara, R. H. & Ferre, A. L. T-Cell Biology in the Female Reproductive Tract: Relevance to HIV Infection. *Am J Reprod Immunol* **95**, e70259 (2026). https://doi.org/10.1111/aji.70259

43 Jameson, S. C. & Masopust, D. Diversity in T cell memory: an embarrassment of riches. *Immunity* **31**, 859-871 (2009). https://doi.org/10.1016/j.immuni.2009.11.007

44 Thomas, P. G. Entering the Age of Specificity in T Cell Immunity. *Immunol Rev* **343**, e70184 (2026). https://doi.org/10.1111/imr.70184

45 Kovats, S. Estrogen receptors regulate innate immune cells and signaling pathways. *Cell Immunol* **294**, 63-69 (2015). https://doi.org/10.1016/j.cellimm.2015.01.018

46 Guan, X. *et al.* Androgen receptor activity in T cells limits checkpoint blockade efficacy. *Nature* **606**, 791-796 (2022). https://doi.org/10.1038/s41586-022-04522-6

47 Henze, L., Schwinge, D. & Schramm, C. The Effects of Androgens on T Cells: Clues to Female Predominance in Autoimmune Liver Diseases? *Front Immunol* **11**, 1567 (2020). https://doi.org/10.3389/fimmu.2020.01567

48 Brown, M. A. & Su, M. A. An Inconvenient Variable: Sex Hormones and Their Impact on T Cell Responses. *J Immunol* **202**, 1927-1933 (2019). https://doi.org/10.4049/jimmunol.1801403

49 Phong, K. T., Song, S., Kim, E. A., Conrad, D. N. & Gartner, Z. J. Single cell RNA-sequencing reveals that testosterone reduces estrogen signaling in the healthy human mammary gland. *J Mammary Gland Biol Neoplasia* **31** (2026). https://doi.org/10.1007/s10911-026-09605-y

50 Shao, X. *et al.* Testosterone Represses Estrogen Signaling by Upregulating miR-22: A Mechanism for Imbalanced Steroid Hormone Production in Preeclampsia. *Hypertension* **69**, 721-730 (2017). https://doi.org/10.1161/HYPERTENSIONAHA.116.08468